PHILOSOPHICAL TRANSACTIONS OF THE ROYAL SOCIETY A MATHEMATICAL, PHYSICAL & ENGINEERING SCIENCES

Dynamical Theory of Electron Diffraction for the Electron Microscopic Image of Crystal Lattices II. Image of Superposed Crystals (Moire Pattern)

H. Hashimoto, M. Mannami and T. Naiki

Phil. Trans. R. Soc. Lond. A 1961 **253**, 490-516
doi: 10.1098/rsta.1961.0007

DYNAMICAL THEORY OF ELECTRON DIFFRACTION FOR THE ELECTRON MICROSCOPIC IMAGE OF CRYSTAL LATTICES

II. IMAGE OF SUPERPOSED CRYSTALS (MOIRÉ PATTERN)

By H. HASHIMOTO,† M. MANNAMI‡ AND T. NAIKI†

(*Communicated by A. H. Cottrell, F.R.S.—Received 27 May 1960*)

[Plates 7 and 8]

CONTENTS

The dynamical theory of electron diffraction is applied to the interpretation of electron microscopic images of moiré patterns. Two cases often observed are treated. One is the case where two plate-shaped crystals are superposed closely without a vacuum layer between them and another is the case where two crystals are superposed with a vacuum layer between them. Resolved lattice images of two superposed crystals are also interpreted. The intensity profiles of the images vary with the thicknesses of the crystals and vacuum layer and with the deviation from the Bragg angle. The shifts of the fringes and anomalies of the contrast which are expected from the present theory were observed in the electron microscopic images of moiré patterns of cupric sulphide, palladium-gold and platinum-phthalocyanine. The relation between moiré patterns and crystal structure is also discussed.

1. Introduction

In the electron microscopic image of superposed crystals, uniformly spaced fringe systems have been reported by several workers recently. Mitsuishi, Nagasaki & Uyeda (1951) first observed moiré patterns for graphite crystals and after their observation, Seki (1951, 1953) observed the same for the mineral sericite, Bernard & Pernoux (1953) for lead iodide and molybdenum oxide, Hillier (1954) for iron oxide, Dowell, Farrant & Rees (1956, 1957) for MoO_3 smoke crystals, Hashimoto & Uyeda (1957) for copper sulphide, Pashley Menter & Bassett (1957) for metal crystals, Goodman (1957) for boron nitride, Dawson &

† Physical Institute, Kyoto Technical University, Kyoto, Japan
‡ Physical Institute, Kyoto University, Kyoto, Japan.

Follett (1959) and Izui (1959) for graphite. Rang (1953) and Möllenstedt & Duker (1953) observed essentially moiré fringe effects between two lamellae of mica and molybdenum sulphide. There are two kinds of interpretation of this fringe system; one is a double-diffraction interpretation which was first proposed by Mitsuishi, Nagasaki & Uyeda (1951) and by Seki (1953), and another is an interpretation which considers a moiré pattern as representing the regions of matching and mismatching between two rotated overlapping lattices and was proposed by Hillier (1954). These were shown to be closely linked by Dowell *et al.* (1956, 1957). They have shown that the fringes are in fact moiré patterns, the formation of which depends upon the occurrence of double diffraction.

The moiré pattern, however, became considerably more important when it was realized that an edge dislocation in one of the lattices is imaged in the moiré pattern. This was shown independently by Hashimoto & Uyeda (1957) and by Pashley, Menter & Bassett (1957) using rotation moiré patterns and parallel moiré patterns respectively. In both cases, an extra terminating half-line appeared on the moiré pattern corresponding to a dislocation in one of the lattices. Hashimoto (1958) has shown that the spacing anomalies and stacking faults in the lattices are also revealed in rotation moiré patterns. Bassett, Menter & Pashley (1958), by superposing thin films which were prepared separately and by using two epitaxially grown films, examined the moiré pattern. They discussed the mode of formation of moiré patterns in detail and the effect of a general dislocation on the moiré pattern.

The relation between the moiré pattern and the crystal structure was first discussed by Dowell *et al.* (1956) in a certain limiting case. They consider the case of two identical overlapping crystals with small rotational misorientation in terms of the kinematical theory of electron diffraction and have pointed out that the pattern may represent the Patterson function of the crystal projection.

More general and detailed theoretical studies have been done by Cowley (1959) and Cowley & Moodie (1959) by approximating the crystals to phase gratings. Cowley (1959) discussed the contrast of the images of two thin superposed crystals and suggested that the background intensity, the contrast and the phase of the moiré pattern will vary widely with the structure factors, crystal thicknesses and excitation errors for the two crystals. Cowley & Moodie (1959) treated the case where the two thin crystals were separated by an arbitrary distance. They discussed the contrast of moiré patterns from separated, rotated and unlike pairs of crystals. They also discussed possible applications of moiré patterns to structure analysis.

For the crystals thicker than several tens of ångströms, the dynamical interaction of electrons with a crystal cannot be disregarded. The present authors, then, have interpreted the intensity distribution of several moiré patterns by using the dynamical theory of electron diffraction developed first by Bethe (1928). Under the two-beam approximation, the cases where the two plate-shaped crystals are superposed with and without a vacuum layer between them have been treated. Absorption of electrons by the crystals and divergence of the illuminating system are neglected because the effect of them can be estimated from the previous considerations of the image of single crystals (part I).

Theoretical interpretations are compared with observed images and the application of moiré patterns to crystal structure analysis is also discussed.

The notation used in this paper is similar to those in the preceding paper (part I).

PHILOSOPHICAL TRANSACTIONS OF THE ROYAL SOCIETY A MATHEMATICAL, PHYSICAL & ENGINEERING SCIENCES

2. Close superposition of two plate-shaped crystals

(*a*) *Wave functions of moiré patterns*

As was pointed out by Mitsuishi *et al.* (1951), Seki (1951) and Dowell *et al.* (1956, 1957), the moiré pattern in the electron microscopic image of crystal lattices is formed as the interference fringes of the transmitted primary wave and the secondary wave successively reflected by the lattice planes in two superposed crystals. In this section, the wave function and intensity distribution corresponding to the well-focused image by an ideal lens and axial illumination are derived. As the first step of this interpretation, we treat the case where two crystals A and B with different thicknesses Z_A and Z_B are superposed closely with a small rotation angle ϵ. The surfaces of crystals A and B are named a, b, and c, d respectively. In the present case, the b surface coincides with the c surface.

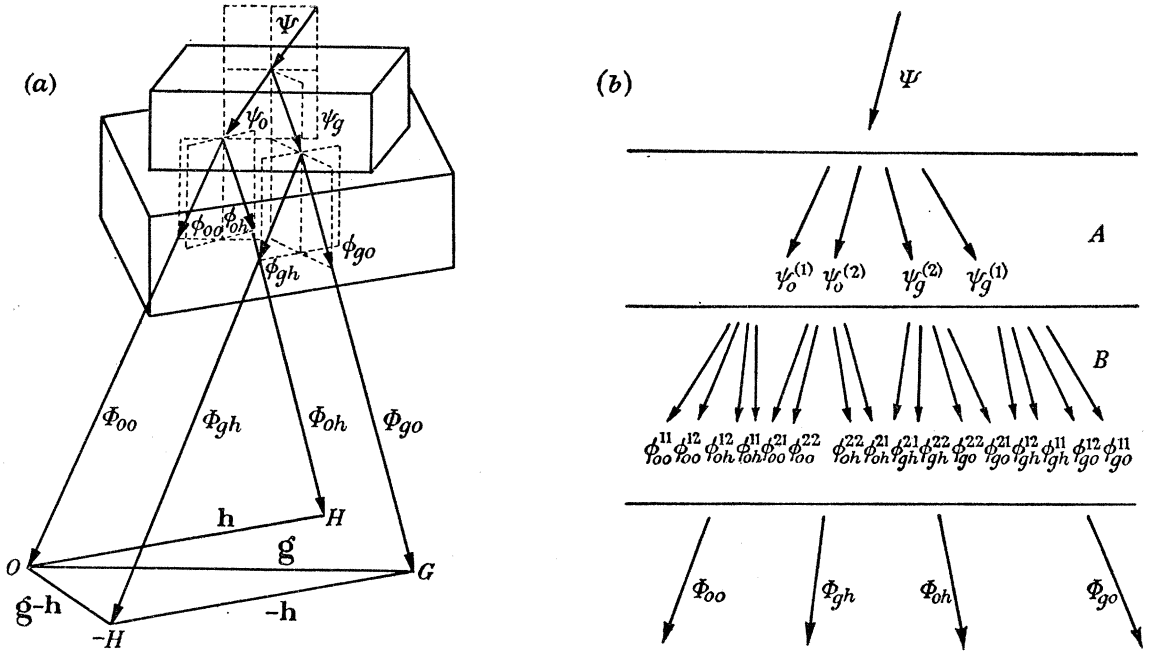

FIGURE 1. (*a*) The dispositions of the two crystals and the paths of the electron waves; (*b*) waves in vacuum and the crystals.

When a plane wave

$$\Psi(\mathbf{r}) = \Psi \exp \mathbf{j}(\mathbf{K}\cdot\mathbf{r}), \tag{2·1}$$

where $\mathbf{j} = 2\pi\sqrt{-1}$ enters a crystal A through surface a and one of the lattice planes $\mathbf{g}$ of the crystal is at the Bragg angle, four waves $\psi_0^1(\mathbf{r})$, $\psi_0^2(\mathbf{r})$, $\psi_g^1(\mathbf{r})$ and $\psi_g^2(\mathbf{r})$ are formed in crystal A. As shown in equations (10) and (15) of part I, they are expressed as

$$\psi_l^i(\mathbf{r}) = \psi_l^i \exp \mathbf{j}(\mathbf{k}_l^i\cdot\mathbf{r}), \tag{2·2}$$

where $l = 0, g$; $i = 1, 2$ and

$$\psi_0^i = \frac{C^1C^2}{C^1 - C^2}\frac{(-1)^i}{C^i}\Psi \exp \mathbf{j}(\mathbf{K} - \mathbf{k}_0^i\cdot\mathbf{R}_a), \tag{2·2a}$$

$$\psi_g^i = C^i\psi_0^i.$$

It can easily be known that each of the four waves in crystal A forms four waves in the crystal B when they enter crystal B and are reflected by lattice planes h and $-h$ respectively.

Therefore, 16 waves are formed in crystal B. They are expressed as

$$\left.\begin{aligned}\phi^{ij}_{l0}(\mathbf{r}) &= \phi^{ij}_{l0}\exp \mathbf{j}(\mathbf{k}^{ij}_{l0}\cdot\mathbf{r}),\\ \phi^{ij}_{lh}(\mathbf{r}) &= \psi^{ij}_{lh}\exp \mathbf{j}(\mathbf{k}^{ij}_{lh}\cdot\mathbf{r}),\end{aligned}\right\} \tag{2·3}$$

where $j = 1, 2$. When these 16 waves pass out to the vacuum it is apparent that they become 4 waves, because the exit surface is parallel to the entrance surface. They are expressed as

$$\left.\begin{aligned}\Phi_{l0}(\mathbf{r}) &= \Phi_{l0}\exp \mathbf{j}(\mathbf{K}_{l0}\cdot\mathbf{r}),\\ \Phi_{lh}(\mathbf{r}) &= \Phi_{lh}\exp \mathbf{j}(\mathbf{K}_{lh}\cdot\mathbf{r}).\end{aligned}\right\} \tag{2·4}$$

The dispositions of the two crystals A and B and the paths of the electron waves are illustrated in figure 1.

The dispersion surface construction which determines wave vectors and the ratio of the amplitudes of primary and reflected waves is illustrated in figure 2. The dispersion surface construction for the crystal A is the same as that shown in figure 2 of part I. For the crystal B, however, two dispersion surfaces have to be constructed, because the two primary waves ϕ_{00} and ϕ_{g0} in the crystal B advance to O and G, and are reflected by the h and $-h$ plane respectively.

The wave points and corresponding wave vectors in the crystals for a given wave vector $\mathbf{K}$ *in vacuo* are determined by the requirement of tangential continuity of the wave vectors on the crystal surface. Wave points obtained by the requirement of tangential continuity are shown in figure 2.

The amplitudes ψ^{ij}_{l0}, ψ^{ij}_{lh}, Φ_{l0} and Φ_{lh} are determined in terms of Ψ by the boundary conditions on the plane b $(= c)$ and d. As was pointed out in part I, in transmission electron microscopy the waves enter the crystal nearly normal to the surface. The normal components of all wave vectors therefore are large compared with the difference among themselves. In such cases, tangential continuity of wave vectors implies continuity of normal derivatives. Then the boundary conditions on both boundary surfaces are expressed as

$$\left.\begin{aligned}\psi^{i}_{l}(\mathbf{r}_b) &= \phi^{i1}_{l0}(\mathbf{r}_b)+\phi^{i2}_{l0}(\mathbf{r}_b)\\ 0 &= \phi^{i1}_{lh}(\mathbf{r}_b)+\phi^{i2}_{lh}(\mathbf{r}_b)\end{aligned}\right\} \quad \text{on the } b \text{ plane.} \tag{2·5}$$

$$\left.\begin{aligned}\sum_i(\phi^{i1}_{l0}(\mathbf{r}_d)+\phi^{i2}_{l0}(\mathbf{r}_d)) &= \Phi_{l0}(\mathbf{r}_d)\\ \sum_i(\phi^{i1}_{lh}(\mathbf{r}_d)+\phi^{i2}_{lh}(\mathbf{r}_d)) &= \Phi_{lh}(\mathbf{r}_d)\end{aligned}\right\} \quad \text{on the } d \text{ plane.} \tag{2·6}$$

By referring to equation (15) in part I, we can obtain the following amplitudes from equations (2·2) and (2·5)

$$\left.\begin{aligned}\phi^{i1}_{l0} &= \frac{-C^{i2}_l}{C^{i1}_l-C^{i2}_l}\psi^{i}_{l}\exp \mathbf{j}(\mathbf{k}^{i}_{l}-\mathbf{k}^{i1}_{l0}\cdot\mathbf{R}_b),\\ \phi^{i2}_{l0} &= \frac{C^{i1}}{C^{i1}_l-C^{i2}_l}\psi^{i}_{l}\exp \mathbf{j}(\mathbf{k}^{i}_{l}-\mathbf{k}^{i2}_{l0}\cdot\mathbf{R}_b),\\ \phi^{i1}_{lh} &= \frac{-C^{i1}_l C^{i2}_l}{C^{i1}_l-C^{i2}_l}\psi^{i}_{l}\exp \mathbf{j}(\mathbf{k}^{i}_{l}-\mathbf{k}^{i1}_{l0}\cdot\mathbf{R}_b),\\ \phi^{i2}_{lh} &= \frac{C^{i1}_l C^{i2}_l}{C^{i1}_l-C^{i2}_l}\psi^{i}_{l}\exp \mathbf{j}(\mathbf{k}^{i}_{l}-\mathbf{k}^{i2}_{l0}\cdot\mathbf{R}_b),\end{aligned}\right\} \tag{2·7}$$

where

$$C^{ij}_l = \phi^{ij}_{lh}/\phi^{ij}_{l0}. \tag{2·8}$$

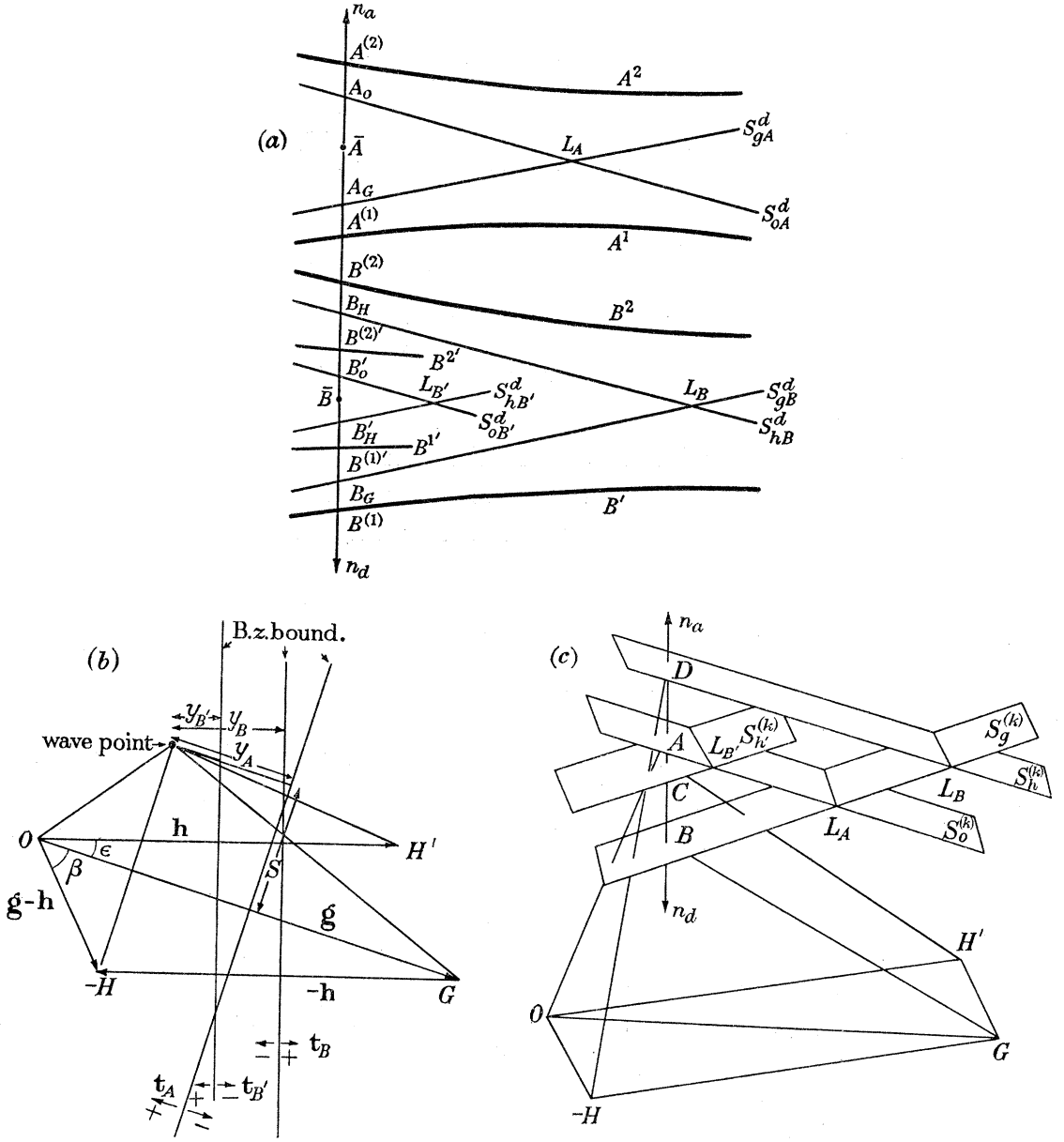

FIGURE 2. Dispersion surface constructions. (*a*) Projection on the plane normal to the crystal surface which passes through *O* and *G*; (*b*) projection on the crystal surface; (*c*) perspective of the kinematic dispersion surface.

O, *G*, *H*, *H'*, the origin and reciprocal lattice points.
A, *B*, *C*, *D*, wave points of vacuum waves.
$A^{(1)}$, $A^{(2)}$, $B^{(1)}$, $B^{(1)\prime}$, $B^{(2)\prime}$, wave points of crystal waves.
A^1, A^2, B^1, B^2, $B^{1\prime}$, $B^{2\prime}$, branches of the dispersion surfaces whose asymptotic surfaces are S^d_{gA}, S^d_{0A}, S^d_{gB}, S^d_{hB}, S^d_{0B}, $S^d_{hB'}$.
n_a, n_d, normal of crystal surfaces.
$\bar{A}$, $\bar{B}$, wave points of mean value of crystal waves.
$S^{(K)}_0$, $S^{(K)}_G$, $S^{(K)}_h$ and $S^{(K)}_{h'}$, spheres of radius $|\mathbf{K}|$ centred on *O*, *G*, *H* and *H'*.
A_0, A_G, B_H, B_G, B'_0, B'_H, intersections of n_a, n_d and S^d_{0A}, S^d_{gA}, S^d_{hB}, S^d_{gB}, $S^d_{0B'}$, $S^d_{hB'}$.

From the condition (2·6) and equations (2·3), (2·4) and (2·7), we can obtain the following amplitudes,

$$\left.\begin{aligned}\Phi_{l0} &= \sum_i \{\phi_{l0}^{i1} \exp \mathbf{j}(\mathbf{k}_{l0}^{i1} - \mathbf{K}_{l0}\cdot\mathbf{R}_d) + \phi_{l0}^{i2} \exp \mathbf{j}(\mathbf{k}_{l0}^{i2} - \mathbf{K}_{l0}\cdot\mathbf{R}_d)\},\\ \Phi_{lh} &= \sum_i \{\phi_{lh}^{i1} \exp \mathbf{j}(\mathbf{k}_{lh}^{i1} - \mathbf{K}_{lh}\cdot\mathbf{R}_d) + \phi_{lh}^{i2} \exp \mathbf{j}(\mathbf{k}_{lh}^{i2} - \mathbf{K}_{lh}\cdot\mathbf{R}_d)\}.\end{aligned}\right\} \tag{2·9}$$

These are rewritten from the equations (2·2a) and (2·7)

$$\begin{aligned}\Phi_{00} = \sum_i \Big\{ &\frac{-C_0^{i2}}{C_0^{i1}-C_0^{i2}} \frac{C^1C^2}{C^1-C^2} \frac{(-1)^i}{C^i} \Psi \exp \mathbf{j}(\mathbf{k}_0^i\cdot\mathbf{Z}_A + \mathbf{k}_{00}^{i1}\cdot\mathbf{Z}_B - \mathbf{K}_{00}\cdot\mathbf{Z}_{AB} - \mathbf{u}\cdot\mathbf{R}_d)\\ &+ \frac{C^{i1}}{C_0^{i1}-C_0^{i2}} \frac{C^1C^2}{C^1-C^2} \frac{(-1)^i}{C^i} \Psi \exp \mathbf{j}(\mathbf{k}_0^i\cdot\mathbf{Z}_A + \mathbf{k}_{00}^{i2}\cdot\mathbf{Z}_B - \mathbf{K}_{00}\cdot\mathbf{Z}_{AB} - \mathbf{u}\cdot\mathbf{R}_d)\Big\},\end{aligned} \tag{2·10}$$

$$\begin{aligned}\Phi_{0h} = \sum_i \Big\{ &\frac{-C_0^{i1}C_0^{i2}}{C_0^{i1}-C_0^{i2}} \frac{C^1C^2}{C^1-C^2} \frac{(-1)^i}{C^i} \Psi \exp \mathbf{j}(\mathbf{k}_0^i\cdot\mathbf{Z}_A + \mathbf{k}_{00}^{i1}\cdot\mathbf{Z}_B - \mathbf{K}_{00}\cdot\mathbf{Z}_{AB} - \mathbf{u}\cdot\mathbf{R}_d)\\ &+ \frac{C_0^{i1}C_0^{i2}}{C_0^{i1}-C_0^{i2}} \frac{C^1C^2}{C^1-C^2} \frac{(-1)^i}{C^i} \Psi \exp \mathbf{j}(\mathbf{k}_0^i\cdot\mathbf{Z}_A + \mathbf{k}_{00}^{i2}\cdot\mathbf{Z}_B - \mathbf{K}_{00}\cdot\mathbf{Z}_{AB} - \mathbf{u}\cdot\mathbf{R}_d)\Big\}.\end{aligned} \tag{2·11}$$

$$\begin{aligned}\Phi_{g0} = \sum_i \Big\{ &\frac{-C_g^{i2}}{C_g^{i1}-C_g^{i2}} \frac{C^1C^2}{C^1-C^2} (-1)^i \Psi \exp \mathbf{j}(\mathbf{k}_0^i\cdot\mathbf{Z}_A + \mathbf{k}_{00}^{i1}\cdot\mathbf{Z}_B - \mathbf{K}_{00}\cdot\mathbf{Z}_{AB} - \mathbf{u}\cdot\mathbf{R}_d)\\ &+ \frac{C_g^{i1}}{C_g^{i1}-C_g^{i2}} \frac{C^1C^2}{C^1-C^2} (-1)^i \Psi \exp \mathbf{j}(\mathbf{k}_0^i\cdot\mathbf{Z}_A + \mathbf{k}_{00}^{i2}\cdot\mathbf{Z}_B - \mathbf{K}_{00}\cdot\mathbf{Z}_{AB} - \mathbf{u}\cdot\mathbf{R}_d)\Big\},\end{aligned} \tag{2·12}$$

$$\begin{aligned}\Phi_{gh} = \sum_i \Big\{ &\frac{-C_g^{i1}C_g^{i2}}{C_g^{i1}-C_g^{i2}} \frac{C^1C^2}{C^1-C^2} (-1)^i \Psi \exp \mathbf{j}(\mathbf{k}_0^i\cdot\mathbf{Z}_A + \mathbf{k}_{00}^{i1}\cdot\mathbf{Z}_B - \mathbf{K}_{00}\cdot\mathbf{Z}_{AB} - \mathbf{u}\cdot\mathbf{R}_d)\\ &+ \frac{C_g^{i1}C_g^{i2}}{C_g^{i1}-C_g^{i2}} \frac{C^1C^2}{C^1-C^2} (-1)^i \Psi \exp \mathbf{j}(\mathbf{k}_0^i\cdot\mathbf{Z}_A + \mathbf{k}_{00}^{i2}\cdot\mathbf{Z}_B - \mathbf{K}_{00}\cdot\mathbf{Z}_{AB} - \mathbf{u}\cdot\mathbf{R}_d)\Big\}.\end{aligned} \tag{2·13}$$

where $\mathbf{Z}_A$, $\mathbf{Z}_B$ and $\mathbf{Z}_{AB}$ are the thicknesses of the crystals A, B and the sum of them, and $\mathbf{R}_d$ is the special case of $\mathbf{r}_d$ where it is normal to the exit surface.

Since the object of this section is to obtain the intensity distribution of well-focused transmission microscopic images theoretically it is sufficient to evaluate the wave function at the point $\mathbf{r}_d$ on the exit surface of the crystal. The moiré pattern of an ordinary electron microscopic image is formed by the interference of two waves $\Phi_{00}(\mathbf{r})$ and $\Phi_{gh}(\mathbf{r})$. The dark-field image of a moiré pattern is formed by the interference of two waves $\Phi_{0h}(\mathbf{r})$ and $\Phi_{g0}(\mathbf{r})$. If the whole wave $\Phi_{00}(\mathbf{r})$, $\Phi_{g0}(\mathbf{r})$, $\Phi_{0h}(\mathbf{r})$ and $\Phi_{gh}(\mathbf{r})$ passes through the aperture of the objective lens and forms the image by mutual interference, the resolved lattice image of two superposed crystals will be observed. The wave function of the moiré pattern in the bright-field image therefore is written from equations (2·10), (2·13) and (2·4):

$$\Phi(\mathbf{r}_d) = \Phi_{00} \exp \mathbf{j}(\mathbf{K}_{00}\cdot\mathbf{r}_d) + \Phi_{gh} \exp \mathbf{j}(\mathbf{K}_{gh}\cdot\mathbf{r}_d). \tag{2·14a}$$

The wave function of the moiré pattern in the dark-field image is written from equations (2·11), (2·12) and (2·4):

$$\Phi_D(\mathbf{r}_d) = \Phi_{0h} \exp \mathbf{j}(\mathbf{K}_{0h}\cdot\mathbf{r}_d) + \Phi_{g0} \exp \mathbf{j}(\mathbf{K}_{g0}\cdot\mathbf{r}_d). \tag{2·14b}$$

The deviation from the Bragg angle is expressed by parameters named resonance errors. These parameters are introduced here. For the crystal A, the resonance error is given by the quantity

$$\overrightarrow{AB} = \overrightarrow{A_0A_G} = 2\mathbf{t}_A \quad \text{or} \quad \overrightarrow{A^{(2)}A^{(1)}} = 2\mathbf{d}_A \tag{2·15}$$

as indicated in figure 2 (*a*), (*c*). For the crystal B, two parameters are introduced, because the transmitted wave $\psi_0(\mathbf{r})$ and reflected wave $\psi_g(\mathbf{r})$ in crystal A enter crystal B in directions differing by an angle 2θ,

$$\overrightarrow{BD} = \overrightarrow{B_G B_H} = 2\mathbf{t}_B \quad \text{or} \quad \overrightarrow{B^{(2)}B^{(1)}} = 2\mathbf{d}_B, \tag{2·16}$$

$$\overrightarrow{AC} = \overrightarrow{B'_0 B_{H'}} = 2\mathbf{t}_{B'} \quad \text{or} \quad \overrightarrow{B^{(2)'}B^{(1)'}} = 2\mathbf{d}_{B'}, \tag{2·17}$$

where a prime (′) refers to the H' plane of crystal B.

From the relation of a hyperbola and its asymptote, it is seen that

$$-d_{A1}d_{A2} = q_A^2, \quad -d_{B1}d_{B2} = q_B^2, \quad -d_{B1'}d_{B2'} = q_{B'}^2, \tag{2·18}$$

$$d_A = \sqrt{(t_A^2+q_A^2)}, \quad d_B = \sqrt{(t_B^2+q_B^2)}, \quad d_{B'} = \sqrt{(t_{B'}^2+q_{B'}^2)}. \tag{2·19}$$

Then

$$\mathbf{d}_{A1}-\mathbf{d}_{A2} = 2\mathbf{d}_A, \quad \mathbf{d}_{B1}-\mathbf{d}_{B2} = 2\mathbf{d}_B, \quad \mathbf{d}_{B1'}-\mathbf{d}_{B2'} = 2\mathbf{d}_{B'}, \tag{2·20}$$

$$\mathbf{d}_{A1}+\mathbf{d}_{A2} = 2\mathbf{t}_A, \quad \mathbf{d}_{B1}+\mathbf{d}_{B2} = 2\mathbf{t}_B, \quad \mathbf{d}_{B1'}+\mathbf{d}_{B2'} = 2\mathbf{t}_{B'}. \tag{2·21}$$

From the relation in figure 2 it is seen that

$$\left.\begin{aligned} y_B - y'_B &= |\mathbf{g}|\cos\epsilon - |\mathbf{h}| = \Delta y, \\ -t_B &= \left\{\frac{t_A}{\tan\theta_{BA}} - S\tan\epsilon\right\}\cos\epsilon\,\tan\theta_{BB} + \tfrac{1}{2}\Delta y\tan\theta_{BB}, \\ t'_B &= \left\{\frac{t_A}{\tan\theta_{BA}} - S\tan\epsilon\right\}\cos\epsilon\,\tan\theta_{BB} - \tfrac{1}{2}\Delta y\tan\theta_{BB}, \end{aligned}\right\} \tag{2·22}$$

where S is the normal distance between a wave point and a plane normal to the crystal surface which passes through O and G and from (1·24) and (1·25) q is given as

$$\left.\begin{aligned} q_A &= Ug/2k\sqrt{(\cos\theta_{0A}\cos\theta_g)} &&= p_A/\sqrt{(\cos\theta_{0A}\cos\theta_g)}, \\ q_B &= U_{-h}/2k\sqrt{(\cos\theta_{gB}\cos\theta_{hB})} &&= p_B/\sqrt{(\cos\theta_{gB}\cos\theta_{hB})}, \\ q_{B'} &= U_{+h}/2k\sqrt{(\cos\theta_{0B}\cos\theta_{hB})} &&= p_{B'}/\sqrt{(\cos\theta_{0B}\cos\theta_{hB})}, \\ p_A &= \frac{Vg}{2\lambda E}, \quad p_B = \frac{V_{-h}}{2\lambda E}, \quad p_{B'} = \frac{V_{+h}}{2\lambda E}. \end{aligned}\right\} \tag{2·23}$$

In terms of $\Delta\theta_{\Delta 0}$, which is an angle of deviation from Bragg angle, the resonance error is written as

$$2t = \kappa\theta_{\Delta 0}\sin 2\theta_B/\cos\theta_g. \tag{1·26}$$

The ratios of amplitudes shown in equations (2·10) to (2·13) are expressed in terms of the parameter d, from the geometry of dispersion surface, as follows:

$$C^i = \psi_g^i/\psi_0^i = d_{Ai}/-p_A, \tag{2·24}$$

$$C_0^{ij} = \phi_{0h}^{ij}/\phi_{00}^{ij} = d_{Bj'}/-p_B, \tag{2·25}$$

$$C_g^{ij} = \phi_{gh}^{ij}/\phi_{g0}^{ij} = d_{Bj}/-p_B. \tag{2·26}$$

It is convenient at this stage to introduce mean values of the wave vectors in the crystal. In figure 2 (*a*), $\bar{A}$, $\bar{B}$, represent wave points for the mean values of the crystal waves.

From the geometry indicated in figure 2, it is seen that

$$\mathbf{k}_0^i = \mathbf{k}_0 + (-1)^i \mathbf{d}_A, \tag{2·27}$$

$$\mathbf{k}_{00}^{ij} = \mathbf{k}_{00} + (-1)^j \mathbf{d}_{B'}, \tag{2·28}$$

$$\mathbf{k}_{g0}^{ij} = \mathbf{k}_{g0} + (-1)^j \mathbf{d}_B = \mathbf{k}_{00} + \mathbf{g} + (-1)^j \mathbf{d}_B, \tag{2·29}$$

$$|\mathbf{K}| = |\mathbf{K}_0| = |\mathbf{K}_{00}|, \tag{2·30}$$

$$\mathbf{K}_{0h} = \mathbf{K}_{00} + \mathbf{h} - 2\mathbf{t}_{B'}, \quad \mathbf{K}_{g0} = \mathbf{K}_{00} + \mathbf{g} - 2\mathbf{t}_A, \quad \mathbf{K}_{gh} = \mathbf{K}_{00} + (\mathbf{g} - \mathbf{h}) + \mathbf{u}, \tag{2·31}$$

$$|\overrightarrow{DA}| = |\mathbf{u}| = |-2\mathbf{t}_A - 2\mathbf{t}_B| = \{|\mathbf{g}| \cos\epsilon - |\mathbf{h}|\} \tan \tfrac{1}{2}\theta_B, \tag{2·32}$$

where $\mathbf{k}_0$, $\mathbf{k}_{00}$, $\mathbf{k}_{g0}$ are mean values for the crystal waves.

Using the values of C^i, C_0^{ij}, C_g^{ij}, $\mathbf{k}_0^i$, $\mathbf{k}_{00}^{ij}$ and $\mathbf{k}_{g0}^{ij}$ we rewrite equations (2·14*a*), (2·14*b*) as follows:

$$\begin{aligned}\Phi(\mathbf{r}_d) = \Psi \exp \mathbf{j}\{&\mathbf{k}_0 \cdot \mathbf{Z}_A + \mathbf{k}_{00} \cdot \mathbf{Z}_B - \mathbf{K}_{00} \cdot (\mathbf{Z}_{AB} - \mathbf{r}_d)\} \\ &\times \Big[\frac{1}{4 d_A d_{B'}} \{d_{A2} \exp(-\mathbf{j}\mathbf{d}_A \cdot \mathbf{Z}_A) - d_{A1} \exp(\mathbf{j}\mathbf{d}_A \cdot \mathbf{Z}_A)\} \\ &\times \{d_{B2'} \exp(-\mathbf{j}\mathbf{d}_{B'} \cdot \mathbf{Z}_B) - d_{B1'} \exp(\mathbf{j}\mathbf{d}_{B'} \cdot \mathbf{Z}_B)\} + \frac{p_A p_B}{4 d_A d_B} \{\exp(-\mathbf{j}\mathbf{d}_A \cdot \mathbf{Z}_A) - \exp(\mathbf{j}\mathbf{d}_A \cdot \mathbf{Z}_A)\} \\ &\times \{\exp(-\mathbf{j}\mathbf{d}_B \cdot \mathbf{Z}_B) - \exp(\mathbf{j}\mathbf{d}_B \cdot \mathbf{Z}_B)\} \exp\{(\mathbf{g} - \mathbf{h} + \mathbf{u}) \cdot \mathbf{r}_d - \mathbf{u} \cdot \mathbf{R}_d\}\Big],\end{aligned} \tag{2·33a}$$

$$\begin{aligned}\Phi_D(\mathbf{r}_d) = \Psi \exp \mathbf{j}\{&\mathbf{k}_0 \cdot \mathbf{Z}_A + \mathbf{k}_{00} \cdot \mathbf{Z}_B - \mathbf{K}_{00} \cdot (\mathbf{Z}_{AB} - \mathbf{r}_d)\} \\ &\times \Big[\frac{p_{B'}}{4 d_A d_{B'}} \{d_{A2} \exp(-\mathbf{j}\mathbf{d}_A \cdot \mathbf{Z}_A) - d_{A1} \exp(\mathbf{j}\mathbf{d}_A \cdot \mathbf{Z}_A)\} \{\exp(-\mathbf{j}\mathbf{d}_{B'} \cdot \mathbf{Z}_B) - \exp(\mathbf{j}\mathbf{d}_{B'} \cdot \mathbf{Z}_B)\} \\ &\times \exp \mathbf{j}\{(\mathbf{h} - 2\mathbf{t}_{B'}) \cdot \mathbf{r}_d + 2\mathbf{t}_{B'} \cdot \mathbf{R}_d\} \frac{p_A}{4 d_A d_B} \{\exp(-\mathbf{j}\mathbf{d}_A \cdot \mathbf{Z}_A) - \exp(\mathbf{j}\mathbf{d}_A \cdot \mathbf{Z}_A)\} \\ &\times \{d_{B2} \exp(-\mathbf{j}\mathbf{d}_B \cdot \mathbf{Z}_B) - d_{B1} \exp(\mathbf{j}\mathbf{d}_B \cdot \mathbf{Z}_B)\} \exp \mathbf{j}\{(\mathbf{g} - 2\mathbf{t}_A) \cdot \mathbf{r}_d + 2\mathbf{t}_A \cdot \mathbf{R}_d\}\Big].\end{aligned} \tag{2·33b}$$

(*b*) *Intensity of moiré patterns*

The current density of electrons is proportional to $\Phi(\mathbf{r})\,\Phi(\mathbf{r})^* |\mathbf{K}| \cos\theta_0$. Then the intensity distribution of electron waves at the exit surface of the crystal corresponding to the bright field image is expressed as

$$I = \Phi(\mathbf{r}_d)\,\Phi(\mathbf{r}_d)^* |\mathbf{K}| \cos\theta_0 = (I_1 + I_2) |\Psi|^2 |\mathbf{K}| \cos\theta_0, \tag{2·34}$$

where†

$$I_1 = \Big\{1 - \frac{q_A^2}{d_A^2} \sin^2 2\pi d_A Z_A\Big\}\Big\{1 - \frac{q_B^2}{d_{B'}^2} \sin^2 2\pi d_{B'} Z_B\Big\} + \Big(\frac{p_A p_B}{d_A d_B}\Big)^2 \sin^2 2\pi d_A Z_A \sin^2 2\pi d_B Z_B, \tag{2·34a}$$

$$I_2 = A \cos 2\pi\{(\mathbf{g} - \mathbf{h}) \cdot \mathbf{r}_d + \alpha\}, \tag{2·34b}$$

$$A = \frac{p_A p_B}{d_A^2 d_B d_{B'}} \sqrt{(B^2 + C^2)} \sin 2\pi d_B Z_B,$$

$$\alpha = \frac{1}{2\pi} \tan^{-1} \frac{B}{C},$$

$$B = 2 t_A d_{B'} \sin^2 2\pi d_A Z_A \cos 2\pi d_{B'} Z_B + d_A t_{B'} \sin 4\pi d_A Z_B \sin 2\pi d_{B'} Z_B,$$

$$C = 2 t_A t_{B'} \sin^2 2\pi d_A Z_A \sin 2\pi d_{B'} Z_B - d_A d_{B'} \sin 4\pi d_A Z_A \cos 2\pi d_{B'} Z_B.$$

† In equation (2·34), $(\mathbf{g} - \mathbf{h} + \mathbf{u}) \cdot \mathbf{r}_d - \mathbf{u} \cdot \mathbf{R}_d$ is replaced by $(\mathbf{g} - \mathbf{h}) \cdot \mathbf{r}_d$, because $\mathbf{u}$ is normal to the crystal surface and the fringe concerned is on the exit surface of the crystal.

Then term I_1, given by equation (2·34a), shows a uniform intensity and represents the background of the image. The terms represented by

$$\{1-(q_A^2/d_A^2)\sin^2 2\pi d_A Z_A\} \tag{2·35a}$$

and

$$\{1-(q_B^2/d_{B'}^2)\sin^2 2\pi d_{B'} Z_B\} \tag{2·35b}$$

are the intensities of the primary waves of crystal A and B respectively and the terms represented by

$$(p_A^2/d_A^2)\sin^2 2\pi d_A Z_A \tag{2·36a}$$

and

$$(p_B^2/d_B^2)\sin^2 2\pi d_B Z_B \tag{2·36b}$$

are the intensities of the reflected waves in crystal A and B respectively. Then the background of the image is formed by adding the products of the two primary waves and the two reflected waves.

The term I_2 represented by equation (2·34b) gives the periodic intensity in the image. From the equation (2·34b) one can easily understand that the image becomes parallel lines which are normal to $(\mathbf{g}-\mathbf{h})$ directions, the intensity profile is represented by a cosine curve, and the period of the fringe $|\mathbf{r}_m|$ is given from equation (2·34b) as

$$|\mathbf{r}_m| = 1/|\mathbf{g}-\mathbf{h}|. \tag{2·37}$$

From the shape of the triangle OGH shown in figure 2 (b), the spacing and rotation angle of the moiré pattern can be seen easily, i.e. the spacing $\mathscr{S}_m$ of the moiré pattern is given by

$$\mathscr{S}_m = 1/|\mathbf{g}-\mathbf{h}| = 1/\sqrt{(|\mathbf{g}|^2+|\mathbf{h}|^2-2|\mathbf{g}||\mathbf{h}|\cos\epsilon)} \tag{2·38}$$

and the rotation angle β of moiré pattern is given by

$$\beta = \sin^{-1}(|\mathbf{h}|\sin\epsilon/|\mathbf{g}-\mathbf{h}|). \tag{2·39}$$

The positions of the lines in the fringe depend on the value of the phase α in equation (2·34b), i.e. on the parameters d (or t) and the thickness Z.

As can be seen in equation (2·34b), the product of $p_A p_B$ decides the sign of the amplitude of the fringe when the thicknesses are constant, i.e. from equation (2·23) the product of the sign of the Fourier coefficients of inner potentials V_g, V_{-h} decides the positions of the maxima and minima of the fringe. If the sign of $V_g \times V_{-h}$ becomes negative the intensity minimum of the fringe changes to a maximum. If these crystals have no centre of symmetry, V_g and V_{-h} are expressed as $|V_g|\exp(-i\varphi_g)$ and $|V_{-h}|\exp(-i\varphi_h)$ where φ_g and φ_h are the phase angles of the crystals. In such a case, equation (2·34b) is rewritten as

$$I_2 = A\cos[2\pi\{(\mathbf{g}-\mathbf{h})\mathbf{r}_d+\alpha\}-\varphi_g-\varphi_h], \tag{2·40}$$

$$A = \frac{|p_A||p_B|}{d_A^2 d_B d_{B'}}\sqrt{(B^2+C^2)}\sin^2 2\pi d_B Z_B.$$

The lines in the fringe, therefore, are shifted by an amount of

$$\mathscr{S}_m(\varphi_g+\varphi_h)/2\pi. \tag{2·41}$$

The intensity distribution of the electron wave at the exit surface of the crystal corresponding to the dark-field image is expressed as

$$I_D = \Phi(\mathbf{r}_d)\,\Phi(\mathbf{r}_d)^*\,|\mathbf{K}|\cos\theta_g = (I_{1D}+I_{2D})\,|\Psi'|^2\,|\mathbf{K}|\cos\theta_g, \tag{2·42}$$

PHILOSOPHICAL TRANSACTIONS OF THE ROYAL SOCIETY A MATHEMATICAL, PHYSICAL & ENGINEERING SCIENCES

where

$$I_{1D} = \left(\frac{p_{B'}}{d_{B'}}\right)^2 \sin^2 2\pi d_{B'} Z_B \left(1 - \frac{q_A^2}{d_A^2} \sin^2 2\pi d_A Z_A\right) + \left(\frac{p_A}{d_A}\right)^2 \sin^2 2\pi d_A Z_A \left(1 - \frac{q_B^2}{d_B^2} \sin^2 2\pi d_B Z_B\right), \tag{2·42a}$$

$$I_{2D} = A_D \cos 2\pi\{(\mathbf{g} - \mathbf{h}) \cdot \mathbf{r}_d + \alpha_D\}, \tag{2·42b}$$

where $A_D = \frac{p_A p_{B'}}{d_A^2 d_B d_{B'}} \sqrt{(B_D^2 + C_D^2)} \sin 2\pi d_{B'} Z_B,$

$$\alpha_D = \frac{1}{2\pi} \tan^{-1} \frac{B_D}{C_D},$$

where $B_D = -d_A t_B \sin 4\pi d_A Z_A \sin 2\pi d_B Z_B - 2t_A d_B \sin^2 2\pi d_A Z_A \cos 2\pi d_B Z_B,$

$$C_D = -d_A d_B \sin 4\pi d_A Z_A \cos 2\pi d_B Z_B + 2t_A t_B \sin^2 2\pi d_A Z_A \sin 2\pi d_B Z_B.$$

The term I_{1D} given by equation (2·42a) shows a uniform intensity and represents the background of the image.

The term I_{2D} represented by equation (2·42b) gives the periodic intensity in the image. The physical meaning of each term follows from the discussion of the equations (2·34) for the bright-field image.

(*c*) *Rotation moiré patterns*

When the two crystals concerned are of the same kind and the relative rotation angle ϵ about an axis normal to the crystal surface is small, the fringe is called a 'rotation moiré pattern'. If the thicknesses of both crystals are the same, the equation (2·34) is written as

$$I = (I_1 + I_2) \, |\Psi'|^2 \, |\mathbf{K}| \cos\theta_0, \tag{2·43}$$

where

$$I_1 = \left(1 - \frac{q^2}{d^2} \sin^2 2\pi dZ\right)^2 + \frac{p^4}{d^4} \sin^4 2\pi dZ, \tag{2·43a}$$

$$I_2 = A \cos 2\pi\{\epsilon g r_{0,-H} + \alpha\}, \tag{2·43b}$$

where $A = \frac{p^2}{d^4} \sin 2\pi dZ \sqrt{(B^2 + C^2)},$

$$\alpha = \frac{1}{2\pi} \tan^{-1} \frac{B}{C},$$

where $B = 2dt \sin 4\pi dZ \sin 2\pi dZ,$

$$C = 2t^2 \sin^3 2\pi dZ - d^2 \sin 4\pi dZ \cos 2\pi dZ,$$

because
$$\left.\begin{aligned} t_A = t'_B = -t_B = t, \quad d_A = d_B = d_{B'} = d, \\ Z_A = Z_B = Z, \quad p_A = p_B = p. \end{aligned}\right\} \tag{2·44}$$

The spacing of the moiré pattern is given by

$$\mathscr{S}_m = \frac{a_g}{2 \sin \frac{1}{2}\epsilon} \doteqdot \frac{a_g}{\epsilon}, \quad \text{where} \quad a_g = \frac{1}{|\mathbf{g}|} \tag{2·45}$$

and the rotation angle is
$$\beta = \sin^{-1} \cos \tfrac{1}{2}\epsilon \doteqdot \tfrac{1}{2}\pi. \tag{2·46}$$

Figure 3 shows how this function varies with d (or t) and dz in the range $-\frac{1}{2} \leqslant \epsilon g.r \leqslant \frac{1}{2}$, i.e. $-a_g/2\epsilon \leqslant r \leqslant a_g/2\epsilon$. This function is periodic in dz and $\epsilon g x$ with period $\frac{1}{2}$ and 1 respectively. The full and dashed curves refer to t positive and negative respectively. The intensity

profile of the fringe of two superposed crystals with the same thickness is given by the condition $Z = C$, where C is constant. As was shown in figure 4 of part I, a line of $Z = C$ passes through the origin $d = 0$ in the diagram of co-ordinates d against dZ. Then the moiré patterns of the crystals with various thicknesses and in various conditions are easily deduced from the curves shown in figure 3.

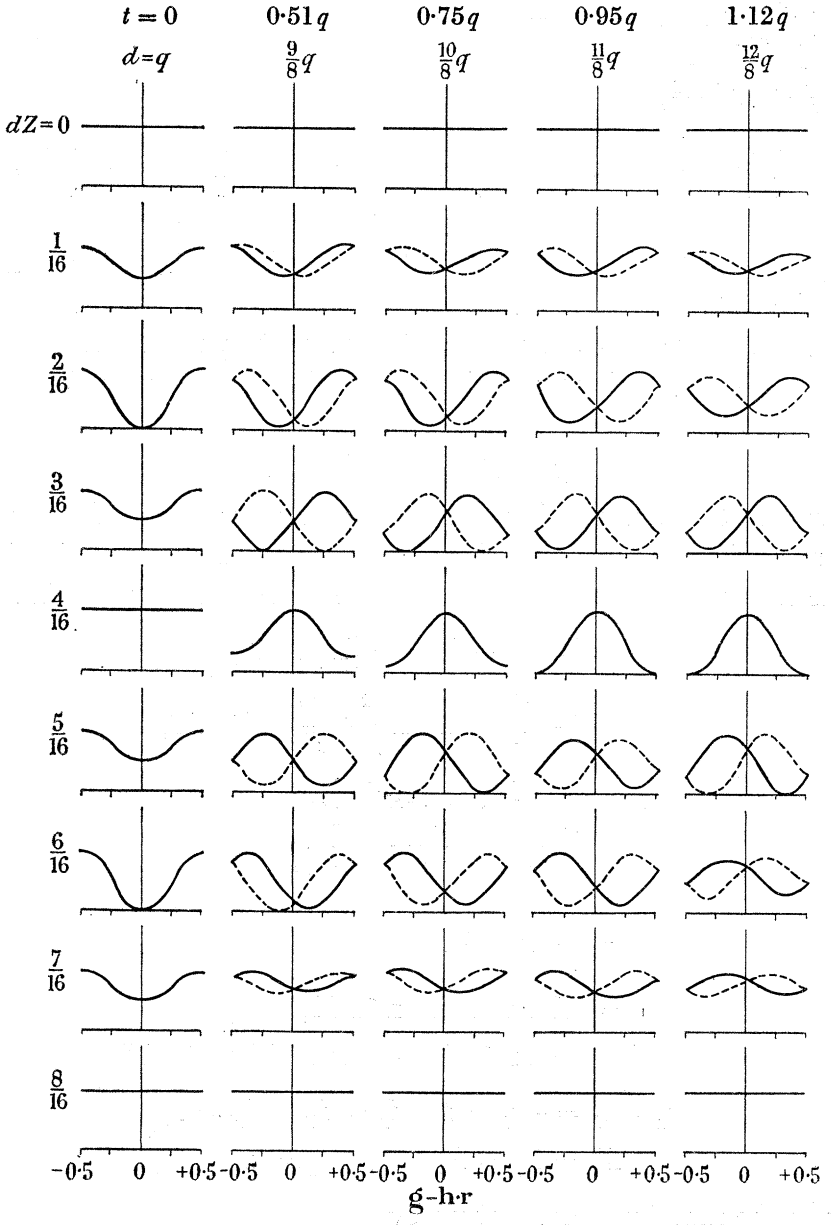

FIGURE 3. Theoretical intensity profile of the bright-field image of the rotation moiré pattern of two superposed crystals with the same thickness Z as a function of $\epsilon g r$ $(= \mathbf{g} - \mathbf{h}\cdot\mathbf{r})$. The different curves correspond to various values of d (or t) and dZ. At $d = q$, $(t = 0)$, i.e. at the Bragg reflecting position, it can clearly be seen that the fringe disappears whenever the thickness becomes $n/4q$ (half of extinction distance). For $d \neq q$, i.e. for deviations from the Bragg angle, the intensity maxima shift gradually with increasing thickness and wherever the thickness becomes $n/2q$, the intensity maxima shift by half the fringe spacing. The full and dashed curves refer to t positive and negative respectively.

PHILOSOPHICAL TRANSACTIONS OF THE ROYAL SOCIETY A MATHEMATICAL, PHYSICAL & ENGINEERING SCIENCES

At the exact Bragg angle ($t = 0$), the intensity profile of the fringe is given by

$$I = \cos^4 2\pi qZ + \sin^4 2\pi qZ - \tfrac{1}{2}\sin^2 4\pi qZ \cos 2\pi\epsilon gr. \qquad (2{\cdot}47)$$

In figure 3 the profiles of the fringe at the exact Bragg angle are given by those on the co-ordinate $d = q$. The intensity of the fringes changes with increase of thickness. The fringes show maximum and zero intensity whenever the thicknesses become $n/8q$, where n is 1, 2, 3, ..., and do not change their position. A schematic diagram of the fringe is illustrated in figure 4 (a). Intensity minima appear on the portion where the centres of symmetry of both crystals are superposed, i.e. for simple crystals the position of superposition of atoms in each crystal.

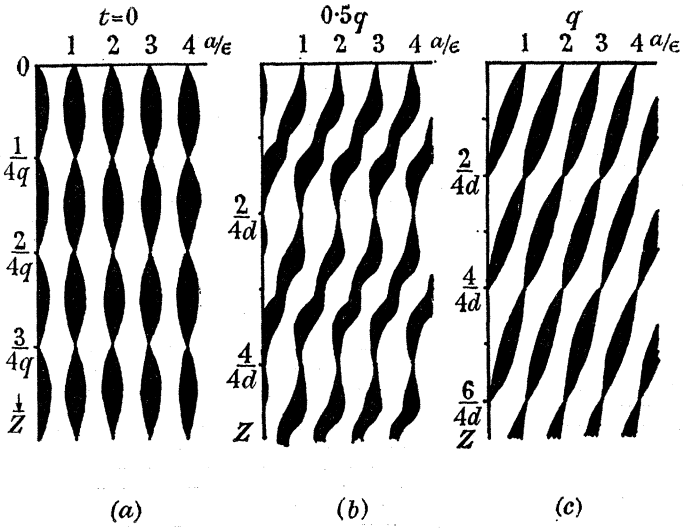

FIGURE 4. Schematic diagram obtained by a study of figure 3 showing the variation of the fringes with thickness and deviation from the Bragg angle: (a) at exact Bragg angle $t = 0$; (b) for a deviation from the Bragg angle $t = 0{\cdot}5q$; (c) $t = q$. $1/2q$ is the extinction distance.

For deviations from the Bragg angle, the profiles of the fringes are given by those with the co-ordinates $t \neq 0$ (or $d \neq q$) in figure 3. The profile and position of the fringe vary both with the deviation from the Bragg angle and with the thickness. In figure 4 (b) and (c), the variations of the fringes due to the increase of thickness are schematically indicated for the case of $t = 0{\cdot}5q$, $t = q$. As can be seen in figure 4, for a deviation from the Bragg angle the fringes appears at a position varying with the thickness; moreover, they do not disappear at the thickness of $n/4d$ ($n = 1, 3, 5, \ldots$).

The moiré patterns of a bent plate-shaped crystal are formed on extinction contour bands. Along the middle line of an extinction contour band the Bragg condition is exactly satisfied and near the edge of the contour, it is not exactly satisfied. Therefore, the variation of the fringes due to deviation from the Bragg angle will be seen on an extinction contour band. As is shown in figure 5, if a crystal is bent into the form of a cylinder the Bragg condition is exactly satisfied at the point A, located in the centre of a contour line, and the Bragg condition is not exactly satisfied at the point B, located at a distance S from the point A. As in the case of equation (37) of part I, distance is proportional to the parameter t, the deviation from the Bragg angle. Therefore it is easy to deduce the moiré fringes on an extinction contour band from figures 3 and 4. In figure 6 fringes of two bent crystals whose mode of bending is

as shown in figure 5, i.e. convex to the incident beam, on an extinction contour band and its subsidiary are schematically illustrated for four different thicknesses. The fringes appear as parallel lines nearly perpendicular to the lattice planes on which double Bragg reflexion has taken place.

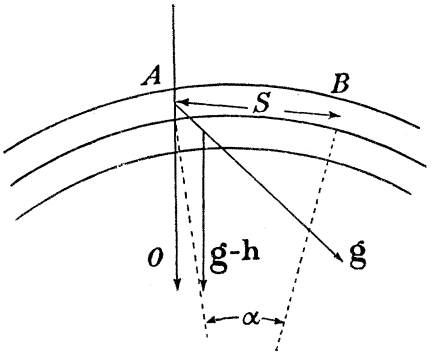

FIGURE 5. Cross-section of two crystals bent into the form of a cylinder indicating the mode of Bragg reflexion.

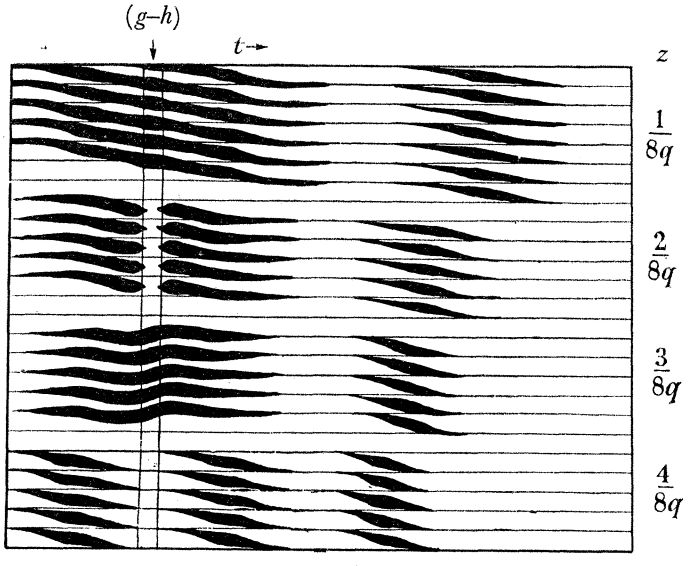

FIGURE 6. Schematic diagram of moiré fringes on an extinction contour band obtained by a study of figures 3 and 4 showing the change of appearance of the fringes of a bent crystal with the mode of bending as shown in figure 5, as the thickness is varied. The lines represent the positions of minima in the intensity profile and the thickness of the line represents the intensity of the profile. The equally spaced thin lines are those connecting the superposition of centres of symmetry of each crystal, where the mass thicknesses in both crystals show a certain maximum or minimum in simple crystals. Thickness $1/2q$ corresponds to an extinction distance.

The lines represent minima in the intensity profile and the thickness of the lines represents the intensity of the lines. The equally spaced thin lines whose spacings are given by a/ϵ represent the position of superpositions of the same kinds of centre of symmetry in each crystal, one of which is adopted as the origin in the present consideration. As is well known, in a crystal with very simple structure, lattice points are located generally at the centre of symmetry. Then if the electron microscopic image of a moiré pattern of the crystal

lattice represented the superposition of the mass thickness in each crystal, the fringes would appear exactly on the thin lines.

As can be seen in this diagram, at the thickness of $1/8q$ which is a quarter of the extinction distance, the fringe along the middle line of the extinction contour band gives maximum contrast and appears exactly on the thin lines, but near the edge of the contour the fringes shift gradually and contrast decreases. The shift of the lines is equal to the spacing of the thin lines near the edges of the contour. On the middle line of the subsidiary extinction contour band, the fringe with maximum intensity appears not on the thin lines but between them. From the centre to each edge of the subsidiary extinction contour band, the lines shift by half of the spacing.

At the thickness $1/4q$, fringes do not appear along the middle line of the extinction contour and the fringes near the edge of the contour shift by an amount equal to half of the spacing and contrast decreases on both edges of the contour.

At the thickness of $3/8q$, the fringe along the middle line of the extinction contour gives maximum contrast and appears exactly on the thin lines but near the edge of the contour the fringes shift gradually in a different way from that for the thickness $1/8q$. At the edge of the contour, however, the shift is recovered and the fringes appear on the thin lines again.

At the thickness $1/2q$ the fringes do not appear along the middle line of the contour and near the edge of the contour the contrast of the fringes increases and the position of the fringes shifts gradually. At the edge of the contour, the shift of the fringes becomes the same as the spacing of the thin lines.

The variation of the fringes on the subsidiary contours for each thickness is nearly the same as for the thickness $1/8q$.

The variation of the fringes between the thickness 0 and $1/2q$ described above is repeated for thicknesses between $1/2q$ and $1/q$, if the absorption is neglected. In general, the fringes have some shifts in the region where the intensity anomaly is observed.

Between two contours, such as the principal and subsidiary contours or contours corresponding to (hkl) and $(\bar{h}\bar{k}\bar{l})$ or (hkl) and $(2h\ 2k\ 2l)$, stepped structures of the fringe are observed.

The intensity distribution of the dark-field image of a rotation moiré pattern for the case that both crystals have the same thickness is given from the equation (2·42) as follows:

$$I_D = (I_{1D}+I_{2D})\,|\Psi'|^2\,|\mathbf{K}|\cos\theta_g, \tag{2·48}$$

where

$$I_{1D} = 2\left(\frac{p}{d}\right)^2 \sin^2 2\pi dZ\left(1-\frac{q^2}{d^2}\sin^2 2\pi dZ\right), \tag{2·48a}$$

$$I_{2D} = A\cos 2\pi(\epsilon g r_{0,-H}), \tag{2·48b}$$

where

$$A = \frac{p^2}{d^4}C_D \sin 2\pi dZ,$$

$$\alpha = \frac{1}{2\pi}\tan^{-1}\frac{B_D}{C_D} = 0,$$

where

$$B_D = 0,$$

$$C_D = -d^2 \sin 4\pi dZ \cos 2\pi dZ - 2t^2 \sin^3 2\pi dZ,$$

because

$$t_A = t'_B = -t_B = t, \quad d_A = d_B = d_{B'} = d,$$

$$Z_A = Z_B = Z, \quad p_A = p_B = p.$$

The spacing of the moiré pattern is given by

$$\mathscr{S}_{mD} = \frac{a_g}{2\sin\frac{1}{2}\epsilon} = \frac{a_g}{\epsilon}, \quad \text{where} \quad a_g = \frac{1}{|\mathbf{g}|} \tag{2·49}$$

and the rotation angle is

$$\beta = \sin^{-1}\cos\tfrac{1}{2}\epsilon \doteqdot \tfrac{1}{2}\pi. \tag{2·50}$$

Figure 7 shows how this function varies with d (or t) and dZ in the range $-\frac{1}{2} \leqslant \epsilon g.r \leqslant \frac{1}{2}$, i.e. $-a_g/2\epsilon \leqslant r \leqslant a_g/2\epsilon$. This function is periodic in dZ and $\epsilon g x$ with period $\frac{1}{2}$ and 1 respectively. By comparing figure 7 with figure 3, it can easily be seen that the intensity maxima of the fringes in the dark-field image do not always appear at the positions of intensity minima of this fringe in the bright-field image.

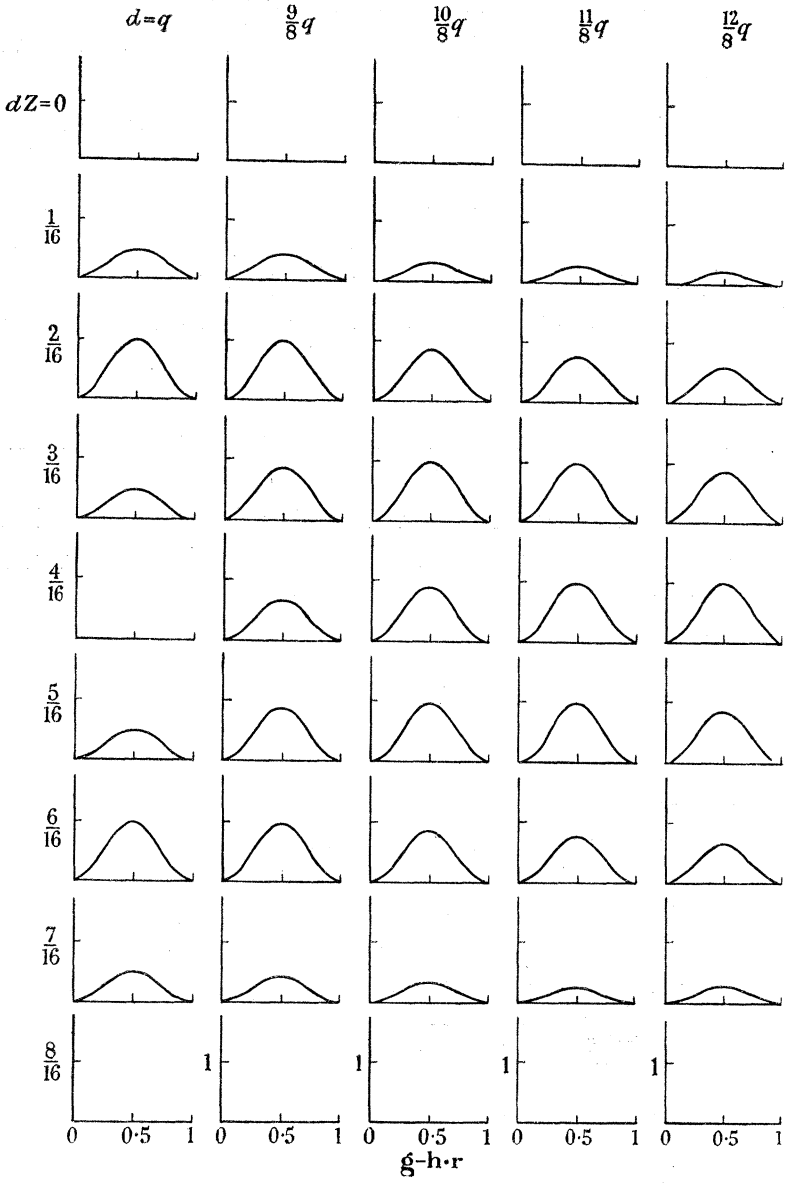

FIGURE 7. Theoretical intensity profile of the dark-field image of the rotation moiré pattern of two superposed crystals with the same thickness Z as a function of $\epsilon g \cdot r (= \mathbf{g} - \mathbf{h} \cdot \mathbf{r})$. The different curves correspond to various values of d (or t) and dZ. The full and dotted curves refer to t positive and negative respectively.

At the exact Bragg angle ($t = 0$), the intensity profile of the fringe is given by

$$I_D = \sin^4 4\pi qZ - \tfrac{1}{2}\sin 2\pi qZ \sin 8\pi qZ \cos 2\pi\epsilon g r_{0,-H}. \tag{2·51}$$

As can be seen in figure 7, at the exact Bragg angle the intensity maxima of the fringe in the dark-field image appears at the same position as the intensity maxima in the bright-field image. Since the contrast of the dark-field electron microscope image of a bent plate-shaped crystal can be deduced from figure 7 as has been discussed in the case of the bright-field image, a detailed discussion will be omitted.

(*d*) *Parallel moiré patterns*

When the two crystals concerned are not of the same kind and the relative rotation angle ϵ is zero, the fringe system is called a 'parallel moiré pattern'. Then the intensity distribution of the parallel moiré pattern is given by the equation (2·34) for the case of $\epsilon = 0$.

The spacing of the moiré pattern can be found from equation (2·38) as

$$\mathscr{S}_m = \frac{1}{|\mathbf{g}| - |\mathbf{h}|} = \frac{a_g a_h}{a_h - a_g}, \quad \text{where} \quad a_g = \frac{1}{|\mathbf{g}|}, \quad a_h = \frac{1}{|\mathbf{h}|}, \tag{2·52}$$

and the rotation angle of the moiré pattern is given from equation (2·39) by

$$\beta = 0. \tag{2·53}$$

In order to know the intensity distribution of a parallel moiré pattern, numerical calculation has been carried out for the case of a film of palladium on gold.

In order to simplify the numerical calculation it is assumed that the thicknesses of the films are the same.

Figure 8 shows how the intensity distribution varies with d_{Pd} (or t_{Pd}) and $d_{\mathrm{Pd}}Z$ in the range

$$0 \leqslant (\mathbf{g} - \mathbf{h}) \cdot \mathbf{r} \leqslant 1, \quad \text{i.e.} \quad 0 \leqslant r \leqslant \frac{a_g a_h}{a_g - a_h}.$$

The variation of the intensity profile is not as simple as in the case of a 'rotation moiré pattern'. Though the thicknesses and orientations of both films are the same, the extinction distances of electron waves and the orders of deviation from the Bragg angle are different for each crystal. Then, even if the thickness of each film is given by $Z = 1/2d_{\mathrm{Pd}}$ this is not equivalent to $1/2d_{\mathrm{Au}}$ and even if the palladium film is at the exact Bragg angle ($t_{\mathrm{Pd}} = 0$), the gold film is not as can be seen from the equation (2·22).

As the mode of the fringes is determined by the combination of the configurations of both crystals it is quite natural that the fringes have a complicated structure. If a film consisting of layers of palladium and gold bends into the form of a cylinder as shown in figure 5, the variation of the moiré pattern due to the deviation from the Bragg angle can be seen at the same time. Figure 9 shows the variations of the fringes for three different thicknesses. The fringes appear as parallel lines perpendicular to the $(\mathbf{g}-\mathbf{h})$ direction.

The lines represent minima in the intensity profile and the thickness of the lines represents the intensity of the lines. Equally spaced thin lines whose spacing is given by $a_g a_h/(a_g - a_h)$ represent the superpositions of the same kinds of centres of symmetry in each crystal, one of which is adopted as the origin in the present consideration. Thin lines, therefore, indicate

the positions where the mass thicknesses in both crystals show certain maximum or minimum in simple crystals.

At the thickness $1/8q$, the fringes along the middle line of the extinction contour band (of palladium) have strong contrast, but away from the middle line the fringes have greater

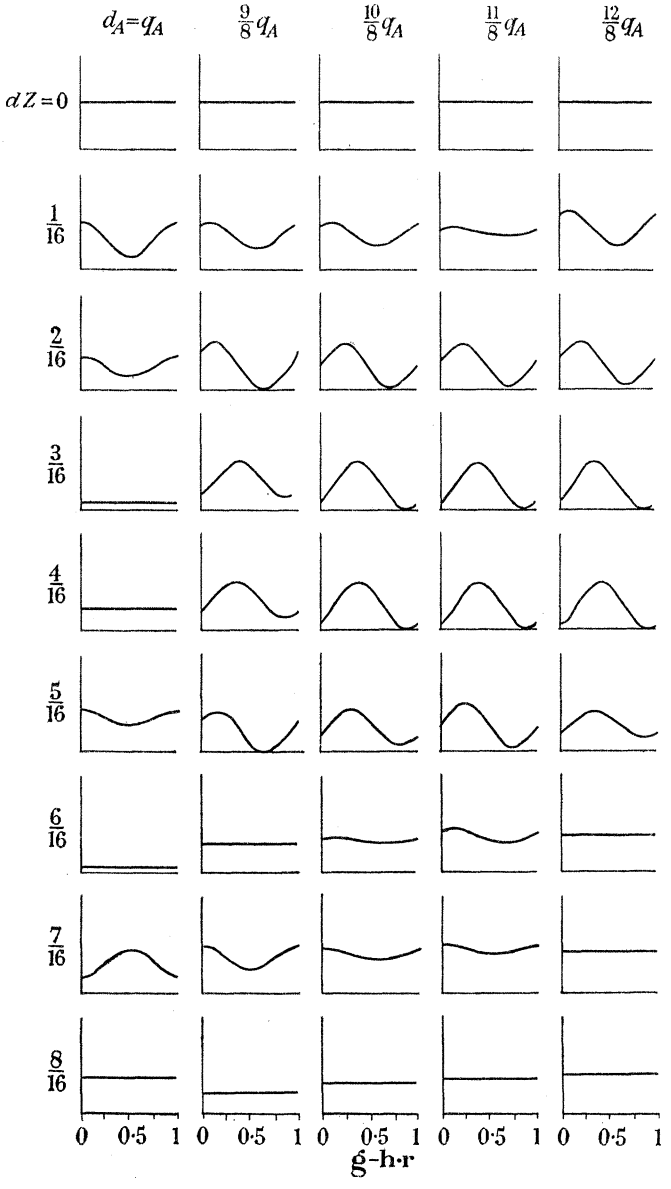

FIGURE 8. Theoretical intensity profile of the bright-field image of the parallel moiré pattern formed by the superposition of a palladium film on a gold film. The thicknesses of the films are the same. The different curves correspond to various values of d (or t) and dZ of the palladium film.

spacing and smaller contrast, and near the edge of the contour the fringes again have strong contrast. At the edge of the contour the fringes have small contrast and increased spacing.

At the thicknesses $2/8q$ and $3/8q$, the fringes do not appear along the middle lines of the extinction contours and the fringes near the edges of the contours have slightly increased spacings.

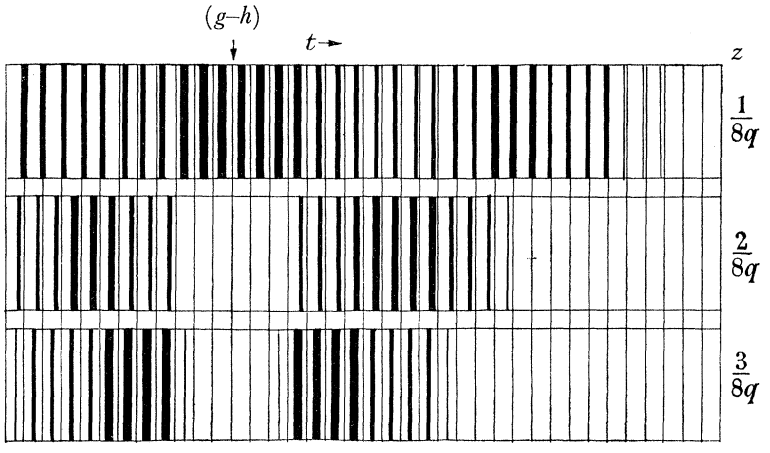

FIGURE 9. Schematic diagram of the parallel moiré pattern formed by the superposition of a palladium film on a gold film of the same thickness showing the change of appearance. An arrow indicates the position of the palladium film at the exact Bragg angle. Thickness $1/4q$ corresponds to half of an extinction distance of the electron wave in a palladium crystal.

3. SUPERPOSITION OF TWO PLATE-SHAPED CRYSTALS WITH VACUUM LAYERS BETWEEN THEM

(a) *Wave function*

Superposition of two films with a vacuum layer between them has often been observed in electron microscopic images. In this section the image of crystals in such a condition is treated.

Let us assume here for simplicity that the wave vectors of the beam are nearly normal to the boundary surface so that the normal components of all wave vectors are large compared with the difference among themselves.

In order to interpret the various kinds of moiré pattern formed by the two crystals with a vacuum layer between them, it is sufficient to interpret the following two kinds of images.

As shown in figure 10 (*a*) and (*b*) the crystal B is tilted to the crystal A with an angle α' and twisted through an angle ϵ. The rectangular co-ordinates xyz are taken as shown in figure 10. Figure 10 (*a*) shows the case where the successive Bragg reflexions take place in the planes nearly parallel to the yz plane. Figure 10 (*b*) shows that successive Bragg reflexions take place in the planes nearly parallel to the xz plane.

In both cases, the primary and the secondary waves *in vacuo* which have passed through the crystal A are given, from the equation (11) of part I as

$$\left.\begin{aligned}\Phi_0(\mathbf{r}) &= \Phi_0 \exp \mathbf{j}(\mathbf{K}_0 \cdot \mathbf{r}),\\ \Phi_g(\mathbf{r}) &= \Phi_g \exp \mathbf{j}(\mathbf{K}_g \cdot \mathbf{r}),\end{aligned}\right\} \qquad (2{\cdot}54a)$$

where Φ_0 and Φ_g are amplitudes and are given by equation (16) in part I. When these two waves enter crystal B through surface (C) and one of the lattice planes h of the crystal is nearly at the Bragg angle to the wave $\Phi_0(\mathbf{r})$, two groups of four waves $\phi^i_{00}(\mathbf{r})$, $\phi^i_{0h}(\mathbf{r})$ and $\phi^i_{g0}(\mathbf{r})$, $\phi^i_{gh}(\mathbf{r})$, $i = 1, 2$, are formed corresponding to the waves $\Phi_0(\mathbf{r})$ and $\Phi_g(\mathbf{r})$.

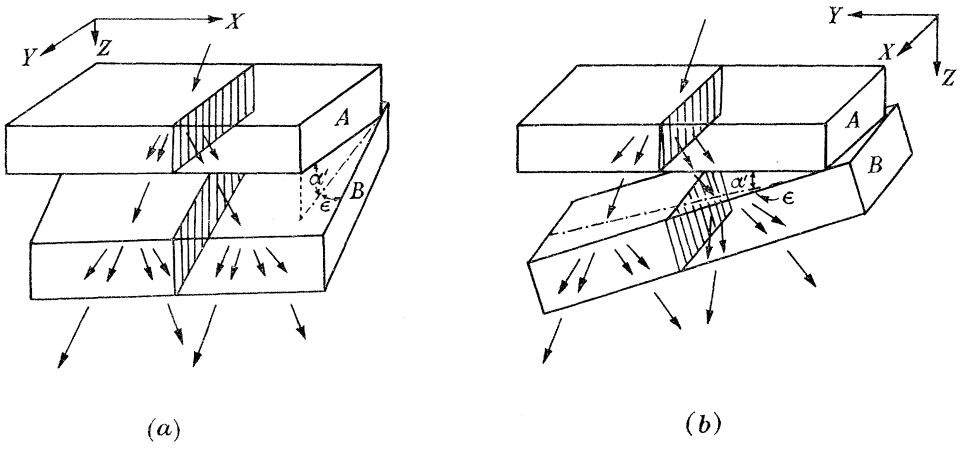

FIGURE 10. Two arrangements for the lattice planes of two plate-shaped crystals superposed with a vacuum layer between them and the waves in the crystal and the vacuum. Rectangular co-ordinates are taken as follows: x and y are parallel and normal directions to the line in which the two crystals A and B meet, and Z is normal to the xy plane. The two kinds of lattice planes are indicated by the yz plane and the xz plane as indicated by shading in (a) and (b) respectively. The xy plane is parallel to surface (a).

They are expressed as

$$\left.\begin{aligned}\phi^i_{00}(\mathbf{r}) &= \phi^i_{00}\exp \mathbf{j}(\mathbf{k}^i_{00}\cdot\mathbf{r}),\\ \phi^i_{0h}(\mathbf{r}) &= \phi^i_{0h}\exp \mathbf{j}(\mathbf{k}^i_{0h}\cdot\mathbf{r}),\\ \phi_{gh}(\mathbf{r}) &= \phi^i_{gh}\exp \mathbf{j}(\mathbf{k}^i_{gh}\cdot\mathbf{r}),\\ \phi_{g0}(\mathbf{r}) &= \phi^i_{g0}\exp \mathbf{j}(\mathbf{k}^i_{g0}\cdot\mathbf{r}).\end{aligned}\right\} \tag{2·55}$$

When these eight waves pass into the vacuum through the surface d it is easy to see that they become four waves, because the surface d is parallel to the entrance surface c. They are expressed as

$$\left.\begin{aligned}\Phi_{00}(\mathbf{r}) &= \Phi_{00}\exp \mathbf{j}(\mathbf{K}_{00}\cdot\mathbf{r}),\\ \Phi_{0h}(\mathbf{r}) &= \Phi_{0h}\exp \mathbf{j}(\mathbf{K}_{0h}\cdot\mathbf{r}),\\ \Phi_{gh}(\mathbf{r}) &= \Phi_{gh}\exp \mathbf{j}(\mathbf{K}_{gh}\cdot\mathbf{r}),\\ \Phi_{g0}(\mathbf{r}) &= \Phi_{g0}\exp \mathbf{j}(\mathbf{K}_{g0}\cdot\mathbf{r}).\end{aligned}\right\} \tag{2·56}$$

The amplitudes ϕ^i_{00}, ϕ^i_{0h}, ϕ^i_{gh}, ϕ^i_{g0}, Φ_{00}, Φ_{0h}, Φ_{gh} and Φ_{g0} are determined in terms of Ψ by the boundary conditions on the planes c and d. In the present interpretation, it is assumed that the electron waves enter the crystals nearly normally. As the tangential continuity of the wave vector implies continuity of normal derivatives, the boundary conditions on c and d surfaces are expressed as

$$\left.\begin{aligned}\Phi_0(\mathbf{r}_c) &= \sum_i \phi^i_{00}(\mathbf{r}_c),\\ 0 &= \sum_i \phi^i_{0h}(\mathbf{r}_c);\\ \Phi_g(\mathbf{r}_c) &= \sum_i \phi^i_{g0}(\mathbf{r}_c),\\ 0 &= \sum_i \phi^i_{gh}(\mathbf{r}_c).\end{aligned}\right\} \quad \text{on the } c \text{ plane,} \tag{2·57}$$

$$\left.\begin{aligned}\sum_i \phi^i_{00}(\mathbf{r}_d) &= \Phi_{00}(\mathbf{r}_d),\\ \sum_i \phi^i_{0h}(\mathbf{r}_d) &= \Phi_{0h}(\mathbf{r}_d),\\ \sum_i \phi^i_{gh}(\mathbf{r}_d) &= \Phi_{gh}(\mathbf{r}_d),\\ \sum_i \phi_{g0}(\mathbf{r}_d) &= \Phi_{g0}(\mathbf{r}_d).\end{aligned}\right\} \quad \text{on the } d \text{ plane.} \tag{2·58}$$

By referring to equations (2·54), (2·55) and (2·56), we can obtain the amplitudes ϕ^i_{00}, ϕ^i_{0h}, ϕ^i_{gh}, ϕ^i_{g0}, Φ_{00}, Φ_{0h}, Φ_{gh} and Φ_{g0}.

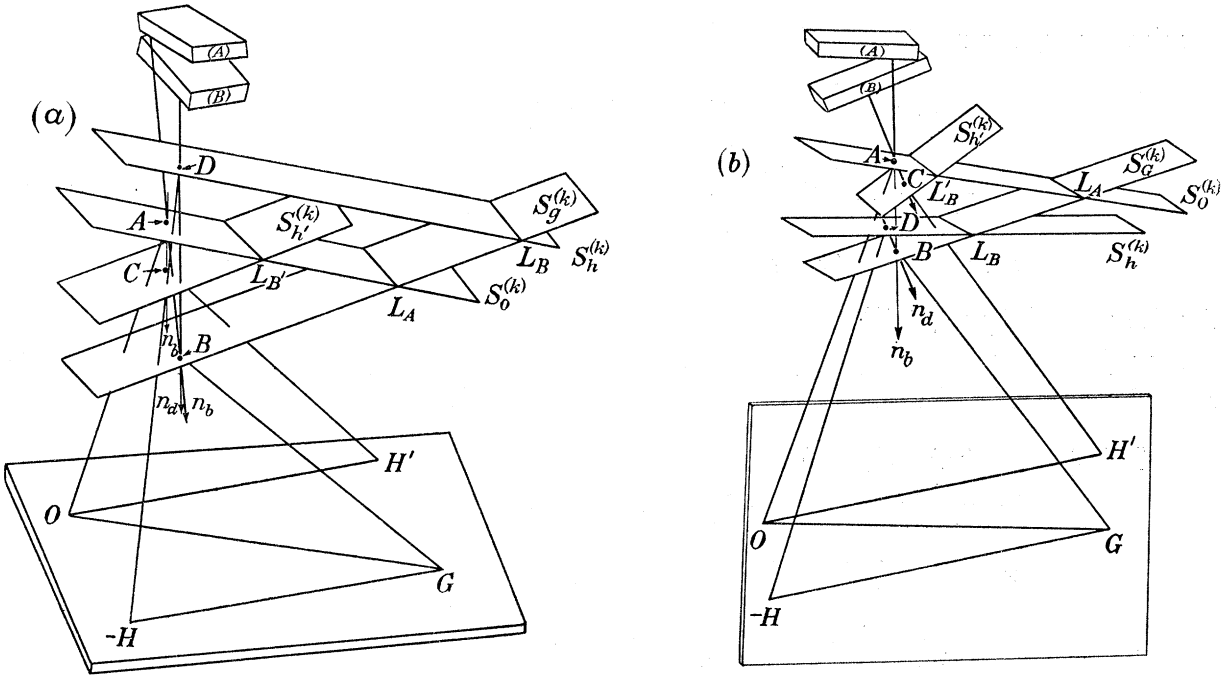

FIGURE 11. The relation between the wave vectors *in vacuo* and the wave points corresponding to the cases of figure 10*a* (*a*) and figure 10*b* (*b*).

Φ_{00} and Φ_{gh} which are the amplitudes of the two waves contributing to the bright-field image of the moiré pattern, are given by

$$\Phi_{00} = \sum_i \left[\frac{-C_0^2}{C_0^1-C_0^2}\frac{C^1C^2}{C^1-C^2}\frac{(-1)^i}{C^i}\Psi^{\mathbf{r}} \exp \mathbf{j}\{\mathbf{k}_0^i\cdot\mathbf{Z}_A+\mathbf{k}_{00}^1\cdot\mathbf{Z}_B-\mathbf{K}_{00}\cdot\mathbf{Z}_{AB}\}\right.$$
$$\left.+\frac{C_0^1}{C_0^1-C_0^2}\frac{C^1C^2}{C^1-C^2}\frac{(-1)^i}{C^i}\Psi^{\mathbf{r}} \exp \mathbf{j}\{\mathbf{k}_0^i\cdot\mathbf{Z}_A+\mathbf{k}_{00}^2\cdot\mathbf{Z}_B-\mathbf{K}_{00}\cdot\mathbf{Z}_{AB}\}\right], \tag{2·59}$$

$$\Phi_{gh} = \sum_i \left[\frac{-C_g^1C_g^2}{C_g^1-C_g^2}\frac{C^1C^2}{C^1-C^2}(-1)^i\Psi^{\mathbf{r}} \exp \mathbf{j}\{\mathbf{k}_0^i\cdot\mathbf{Z}_A+\mathbf{k}_{00}^1\cdot\mathbf{Z}_B-\mathbf{K}_{00}\cdot\mathbf{Z}_{AB}-2\mathbf{t}_A\cdot\mathbf{Z}_v-\mathbf{r}_d\cdot\mathbf{u}\}\right.$$
$$\left.+\frac{C_g^1C_g^2}{C_g^1-C_g^2}\frac{C^1C^2}{C^1-C^2}(-1)^i\Psi^{\mathbf{r}} \exp \mathbf{j}\{\mathbf{k}_0^i\cdot\mathbf{Z}_A+\mathbf{k}_{00}^2\cdot\mathbf{Z}_B-\mathbf{K}_{00}\cdot\mathbf{Z}_{AB}-2\mathbf{t}_A\cdot\mathbf{Z}_v-\mathbf{r}_d\cdot\mathbf{u}\}\right], \tag{2·60}$$

where $C_l^i = \phi^i_{lh}/\phi^i_{l0}$ and z_v is the thickness of vacuum layer. From the dispersion surface constructions shown in figure 11 (*a*) and (*b*) corresponding to the cases shown in figure 10 (*a*) and (*b*) the resonance errors are given by the quantities

$$\vec{AB} = 2\mathbf{t}_A, \quad \vec{BD} = 2\mathbf{t}_B, \quad \vec{AC} = 2\mathbf{t}_{B'} \tag{2·61}$$

and the quantity $\mathbf{u}$ is given by

$$|\mathbf{u}| = |\vec{DA}| = |-2\mathbf{t}_A - 2\mathbf{t}_B|. \tag{2·62}$$

The relations between $2\mathbf{t}_A$, $2\mathbf{t}_B$ and $2\mathbf{t}_{B'}$ are

$$\left.\begin{aligned} -t_B \cos\alpha' &= \left\{\frac{t_A}{\tan\theta_{BA}} - s\tan\epsilon\right\}\cos\epsilon\,\tan\theta_{BB} + \tfrac{1}{2}\Delta y\tan\theta_{BB}, \\ t'_B \cos\alpha' &= \left\{\frac{t_A}{\tan\theta_{BA}} - s\tan\epsilon\right\}\cos\epsilon\,\tan\theta_{BB} - \tfrac{1}{2}\Delta y\tan\theta_{BB}, \\ \Delta y &= |\mathbf{g}|\cos\epsilon - |\mathbf{h}|, \end{aligned}\right\} \tag{2·63}$$

for the case of figure 11 (a) and

$$\left.\begin{aligned} -t_B &= t_A - \frac{\sin(\beta-\theta_{BA})}{2\cos\theta_{BA}}\sqrt{\{(|\mathbf{h}|\sin\alpha'')^2 + (|\mathbf{g}| - |\mathbf{h}|\cos\alpha'')^2\}}, \\ t_{B'} &= t_A - \frac{\sin(\beta+\theta_{BA})}{2\cos\theta_{BA}}\sqrt{\{(|\mathbf{h}|\sin\alpha'')^2 + (|\mathbf{g}| - |\mathbf{h}|\cos\alpha'')^2\}}, \\ \cos\alpha'' &= \cos\alpha'\cos\epsilon, \end{aligned}\right\} \tag{2·64}$$

for the case of figure 11 (b).

By using the relations (2·18) to (2·21) and (2·27) to (2·32) the wave function corresponding to the bright-field image of the moiré pattern is given by

$$\begin{aligned} \Phi_B(\mathbf{r}_d) &= \Phi_{00}(\mathbf{r}_d) + \Phi_{gh}(\mathbf{r}_d) \\ &= \Psi' \exp \mathbf{j}\{\mathbf{k}_0\cdot\mathbf{Z}_A + \mathbf{k}_{00}\cdot\mathbf{Z}_B - \mathbf{K}_{00}\cdot(\mathbf{Z}_{AB} - \mathbf{r}_d)\} \\ &\quad \times\Big[\frac{1}{4d_A d_{B'}}\{d_{A2}\exp(-\mathbf{j}\mathbf{d}_A\cdot\mathbf{Z}_A) - d_{A1}\exp(\mathbf{j}\mathbf{d}_A\cdot\mathbf{Z}_A)\} \\ &\qquad \times\{d_{B2}\exp(-\mathbf{j}\mathbf{d}_{B'}\cdot\mathbf{Z}_B) - d_{B1'}\exp(\mathbf{j}\mathbf{d}_{B'}\cdot\mathbf{Z}_B)\} + \frac{p_A p_B}{4d_A d_B} \\ &\qquad \times\{\exp(-\mathbf{j}\mathbf{d}_A\cdot\mathbf{Z}_A) - \exp(\mathbf{j}\mathbf{d}_A\cdot\mathbf{Z}_A)\}\{\exp(-\mathbf{j}\mathbf{d}_B\cdot\mathbf{Z}_B) - \exp(\mathbf{j}\mathbf{d}_B\cdot\mathbf{Z}_B)\} \\ &\qquad \times\exp\mathbf{j}\{(\mathbf{g}-\mathbf{h}+\mathbf{u})\cdot\mathbf{r}_d - (2\mathbf{t}_A\cdot\mathbf{Z}_v + \mathbf{R}_d\cdot\mathbf{u})\}\Big]. \end{aligned} \tag{2·65}$$

In the present case the focus cannot be adjusted to the whole portion of the exit surface d because of the inclination of crystal B. But, let us assume that the focus is adjusted to a point on the exit surface, which is an intersection point of the normal to the exit surface passing through the origin and the surface, and the interference fringes formed on the exit surface can be projected to the image plane (see figure 11, part I).

(b) *Intensity of moiré patterns*

The intensity distribution of the electron wave at the exit surface of the crystal is expressed from equation (2·65) as

$$I = (I_1 + I_2)\,|\Psi'|^2\,|\mathbf{K}|\cos\theta_0. \tag{2·66}$$

The term I_1 gives uniform intensity and is expressed in the same form as equation (2·34a) and term I_2 gives the periodic intensity and is expressed as

$$I_2 = A\cos 2\pi\{(\mathbf{g}-\mathbf{h}+\mathbf{u})\cdot\mathbf{r}_d - (2\mathbf{t}_A\cdot\mathbf{Z}_v + \mathbf{R}_d\cdot\mathbf{u}) + \alpha\}, \tag{2·67}$$

where A and α have the same form as equation (2·34b). Then the spacing of the moiré pattern is different from that for two closely superposed crystals.

For the case shown in figure 10 (a), equation (2·67) is replaced by

$$I_2 = A\cos 2\pi\{(\mathbf{g}-\mathbf{h})\cdot\mathbf{r}_d - 2\mathbf{t}_A\cdot\mathbf{Z}_v + \alpha\} \tag{2·68}$$

because $\mathbf{u}$ is perpendicular to the image plane. The spacing of the fringes, then, is given by

$$\mathscr{S}_m = \frac{1}{\{|\mathbf{g}-\mathbf{h}| - 2|\mathbf{t}_A|\alpha'\}}. \tag{2·69}$$

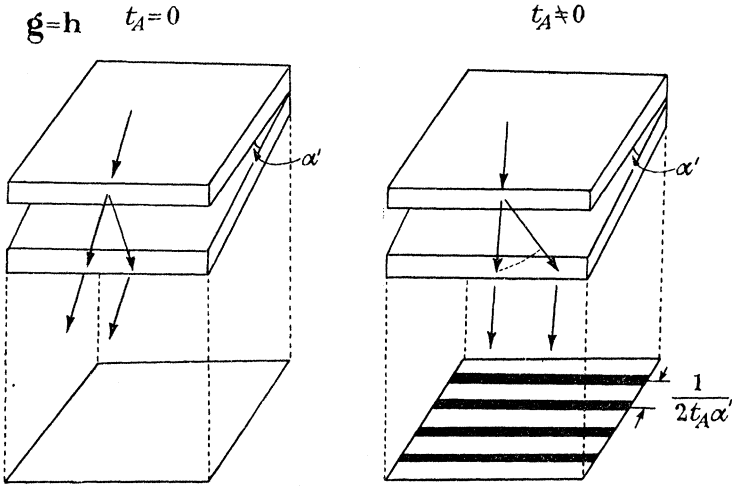

FIGURE 12. Two crystals of the same kind superposed with a wedge-shaped vacuum layer between them and the corresponding electron microscopic image. (a) $t_A = 0$, no fringe. (b) $t_A \neq 0$, fringe with the spacing $1/2t_A\alpha'$.

By comparing equation (2·68) with (2·34b) it can easily be seen that the fringes appear at a position shifted by an amount of $2t_A Z_v$ because of the vacuum layer. If the two crystals are of the same kind and inclined with no twist ($\mathbf{g}=\mathbf{h}$) the spacing of the fringes is given by

$$\mathscr{S}_m = \frac{1}{2t_A\alpha'} = \frac{\lambda\cos\theta_g}{\sin 2\theta_B\alpha'\Delta\theta}. \tag{2·70}$$

Then, the spacing varies with the angle of inclination of the two crystals and the deviation from the Bragg angle. At the exact Bragg angle no fringes can be observed, as shown in figure 12.

For the case shown in figure 10 (b) $\mathbf{u}$ is not perpendicular to the image plane. The spacing of the fringes then is given by

$$\mathscr{S}_m = 1/\{-|\mathbf{g}| + |\mathbf{h}|\cos\alpha' - 2|\mathbf{t}_B|\sin\alpha' + (|\mathbf{h}|\sin\alpha' - 4|\mathbf{t}_A| + 2|\mathbf{t}_B|)\tan\alpha'\}, \tag{2·71}$$

where $\epsilon = 0$.

If both the lattice planes are at the exact Bragg angle ($t_A = t_B = 0$) the spacing of the fringes is given by

$$\mathscr{S}_m = 1/\{(-|\mathbf{g}| + |\mathbf{h}|\cos\alpha') + |\mathbf{h}|\sin\alpha'\tan\alpha'\}. \tag{2·72}$$

The first term of equation (2·72) corresponds to the spacing of the parallel moiré pattern produced by the lattices whose spacings are given by $1/|\mathbf{g}|$ and $1/|\mathbf{h}|\cos\alpha'$ because the spacing of such a moiré pattern is given, from equation (2·52), as

$$\mathscr{S}_m = 1/\{-|\mathbf{g}| + |\mathbf{h}|\cos\alpha'\}. \tag{2·73a}$$

The second term of equation (2·72) corresponds to the spacing of the interference fringes of the electron wave produced by the phase difference due to the vacuum layer between the crystals A and B, because the spacing of such fringes is given, in the present approximation, as

$$\mathscr{S}_m = 1/\{|\mathbf{h}| \sin\alpha' \tan\alpha'\}, \tag{2·73b}$$

where $|\mathbf{h}| = 2\sin\theta_B/\lambda$ (see figure 13).

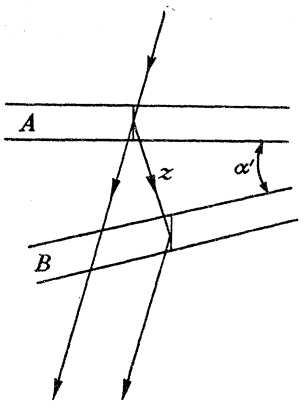

FIGURE 13. Configuration of two crystals superposed with a wedge-shaped vacuum layer between them: $t_A = 0$, $t_B = 0$.

4. RESOLVED LATTICE IMAGE OF TWO SUPERPOSED CRYSTALS

As is pointed out in §2 (*a*), if the whole waves which have passed through two crystals contribute to the imaging, the resolved lattice image of two crystals will be observed. The wave function corresponding to the image is given by

$$\Phi_R(\mathbf{r}) = \Phi_{00}(\mathbf{r}) + \Phi_{0h}(\mathbf{r}) + \Phi_{g0}(\mathbf{r}) + \Phi_{gh}(\mathbf{r}), \tag{2·74}$$

where $\Phi_{00}(\mathbf{r})$, $\Phi_{0h}(\mathbf{r})$, $\Phi_{g0}(\mathbf{r})$ and $\Phi_{gh}(\mathbf{r})$ are given by equations (2·4), (2·10), (2·11), (2·12) and (2·13).

The intensity distribution of the electron wave at the exit surface of the crystal is given by

$$I_R = \Phi_R(\mathbf{r}_d)\,\Phi_R^*(\mathbf{r}_d)\,|\mathbf{K}|\cos\theta_0 = (I_1+I_2+I_3+I_4+I_5)\,|\Psi'|^2\,|\mathbf{K}|\cos\theta_0, \tag{2·75}$$

where

$$\begin{aligned} I_1 &= A, \\ I_2 &= B\sin 2\pi(\mathbf{g}\cdot\mathbf{r}_d+\alpha), \\ I_3 &= C\sin 2\pi(\mathbf{h}\cdot\mathbf{r}_d+\beta), \\ I_4 &= D\sin 2\pi\{(\mathbf{g}-\mathbf{h})\cdot\mathbf{r}_d+\gamma\}, \\ I_5 &= E\sin 2\pi\{(\mathbf{g}-2\mathbf{h})\cdot\mathbf{r}_d+\delta\}, \end{aligned}$$

and A, B, C, D, E, α, β, γ and δ are functions of q_A, q_B, t_A, t_B, $t_{B'}$, Z_A and Z_B.

In figure 14 two kinds of intensity distribution of the resolved lattice image of a rotation moiré pattern can be seen. The angle of rotation is $\alpha = \tan^{-1}\frac{1}{4} \doteqdot 14°$ and the spacing of the lattice is 10 Å. Figure 14 (*a*) shows the intensity distribution at the exact Bragg condition. The moiré fringe appears in the direction normal to the $(\mathbf{g}-\mathbf{h})$ direction and the fringe of spacing 10 Å appears in the direction normal to the $\mathbf{h}$ direction which is the image of the crystal lattice at the exit face. The spacing of the moiré fringes is 20 Å. Figure 14 (*b*) shows

(15)

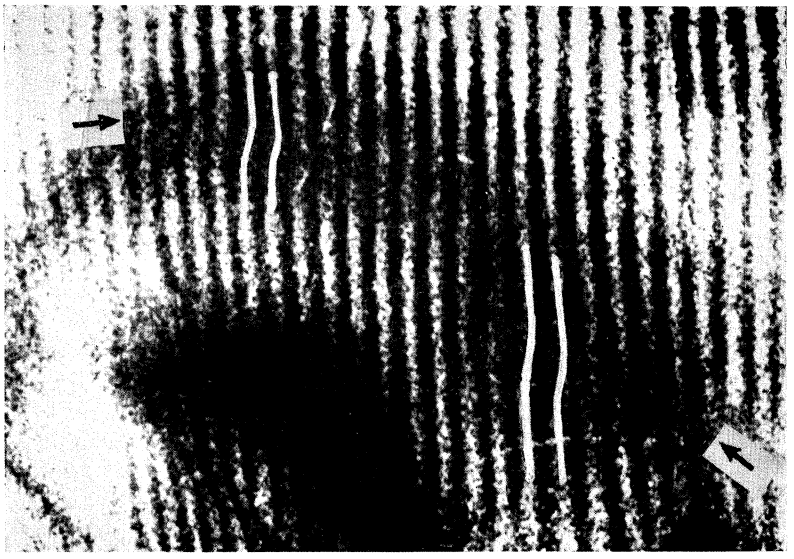

(16)

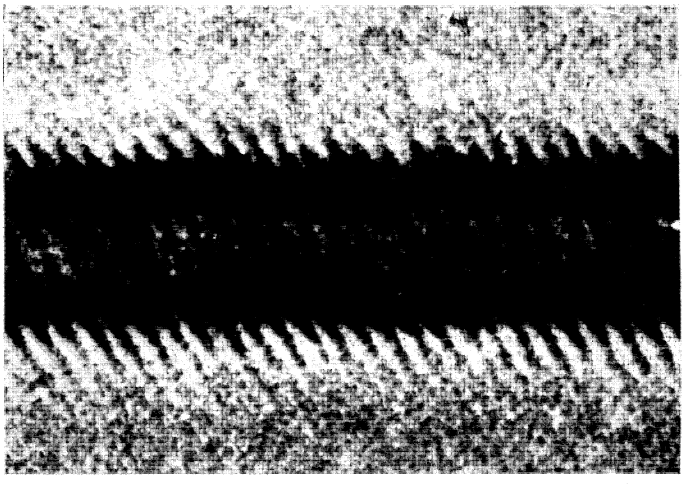

(17)

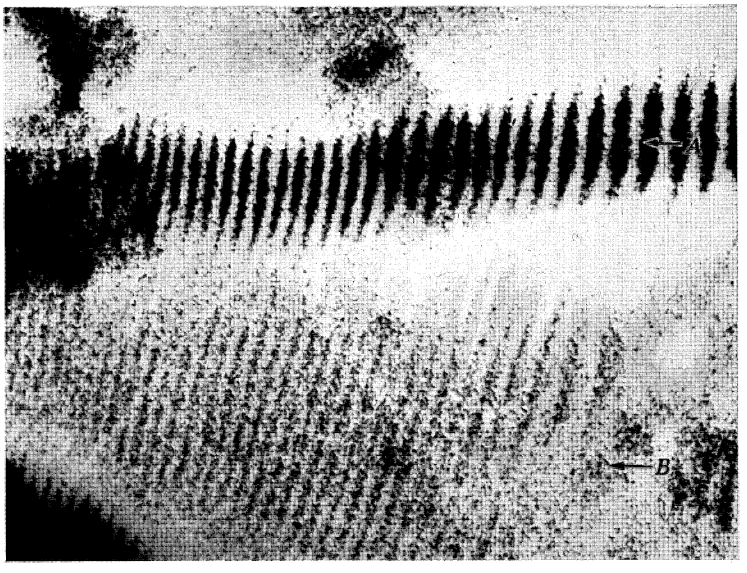

FIGURE 15. Moiré pattern of a cupric sulphide crystal showing the shift of the fringes near the centre of an extinction contour band. See marks ←. (Magn. × 400 000.)

FIGURE 16. Moiré patterns of cupric sulphide crystal on two extinction contour bands 10·0 and $\bar{1}0{\cdot}0$ showing the stepped structure between them. (Magn. × 400 000.)

FIGURE 17. Moiré patterns of a cupric sulphide crystal on a principal contour (*A*) and its neighbouring weak contours (*B*), showing the stepped structure between them. (Magn. × 400 000.)

(*Facing p.* 512)

PHILOSOPHICAL TRANSACTIONS OF THE ROYAL SOCIETY A MATHEMATICAL, PHYSICAL & ENGINEERING SCIENCES

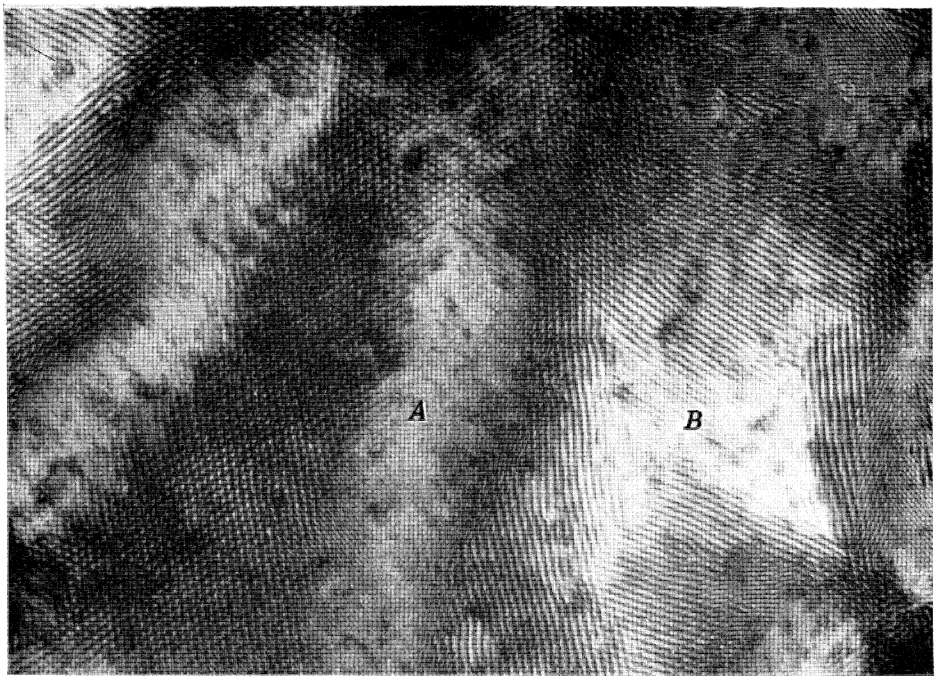

FIGURE 18. Moiré pattern from a specimen consisting of a palladium single crystal grown epitaxially upon a gold single crystal. (Magn. × 300 000.) (Courtesy Bassett, Menter & Pashley 1958.)

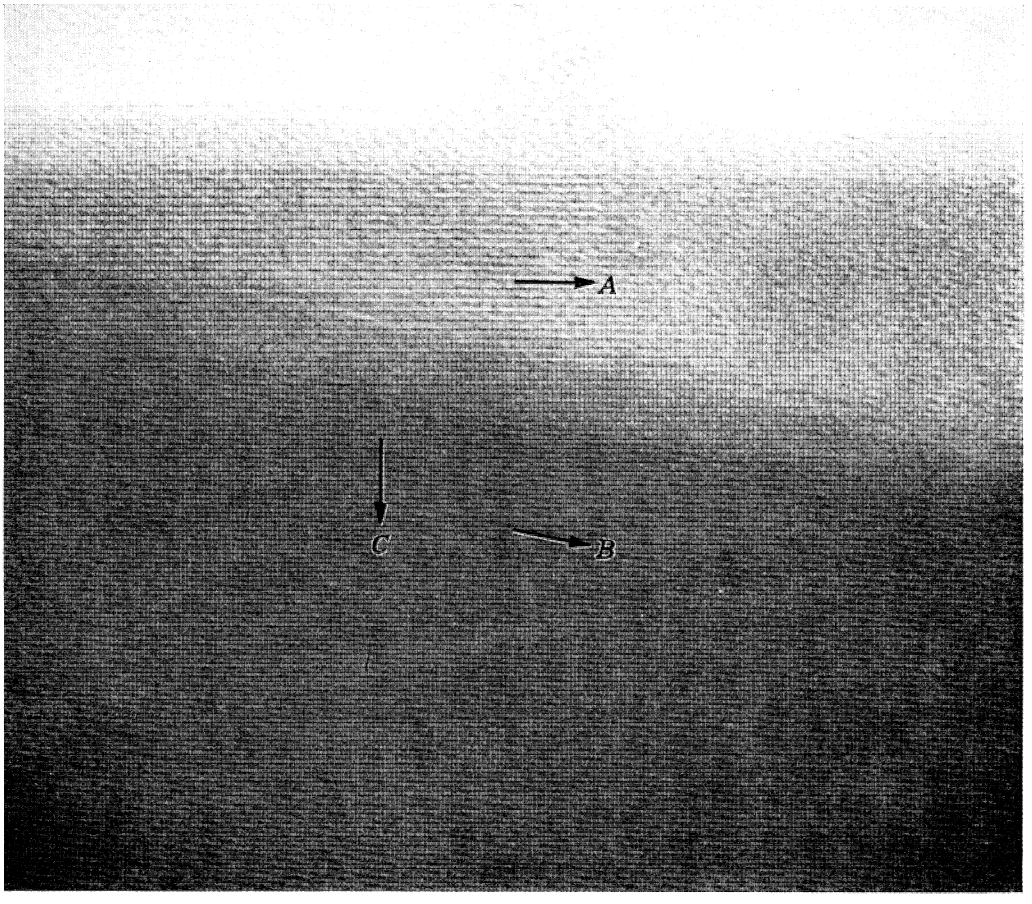

FIGURE 19. Overlapping crystals of platinum phthalocyanine showing crystal lattice fringes resolved and a moiré pattern formed in the region of overlap. (Magn. × 950 000.) (Courtesy Menter 1958.)

PHILOSOPHICAL TRANSACTIONS OF THE ROYAL SOCIETY A MATHEMATICAL, PHYSICAL & ENGINEERING SCIENCES

the intensity distribution for a deviation from the Bragg angle ($d = 9q/8$). Moiré fringes appear in the direction normal to the $(\mathbf{g}-\mathbf{h})$ direction but the direction of the fringes of spacing 10 Å does not appear to be parallel to the lattice planes of either of the two crystals. The intensity of the fringes of spacing 10 Å however, still appears in one direction. The spacing of the moiré fringes becomes 40 Å.

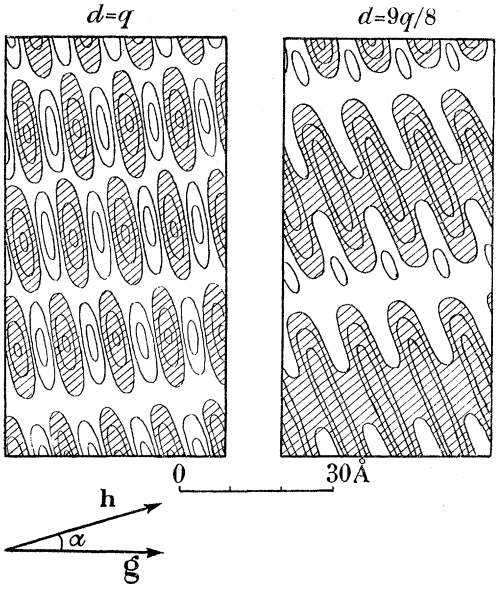

FIGURE 14. Intensity distribution of the resolved lattice image of rotation moiré patterns $|\mathbf{g}| = |\mathbf{h}| = 1/10\text{Å}^{-1}$, $\alpha = \tan^{-1}\frac{1}{4} \doteqdot 14°$, $dZ = \frac{1}{8}$. (*a*) At the Bragg angle $d = q$, (*b*) at the deviation from Bragg angle $d = 9q/8$. The thickness of each crystal is $1/8d$.

5. COMPARISON WITH EXPERIMENT

(*a*) *Rotation moiré patterns*

According to the foregoing interpretation, we should observe the anomalies in contrast of moiré patterns at positions deviating from the Bragg angle.

Figures 15, 16 and 17, plate 7, are electron microscopic images of a cupric sulphide crystal which grew naturally on the surface of copper at 450° C by reaction with saturated sulphur vapour. The diffraction pattern indicates that this crystal consists of two layers twisted with respect to each other. On the extinction contour bands, which are formed by the Bragg reflexion, moiré patterns can be seen clearly.

In figure 15, the fringes of the moiré pattern shift near the centre of an extinction contour band which is indicated by arrows. The mode of the shift of the fringe is similar to that for the thickness between $1/8q$ and $2/8q$ shown in figure 6. Figure 16 shows the moiré pattern on two extinction bands 10·0 and $\bar{1}$0·0. From the small separation of the bands, it can easily be seen that the crystal is severely bent. The moiré pattern, then, appears in a narrow region along the contour bands. A stepped structure between the fringes on the two bands can be clearly seen.

Figure 17 shows the moiré patterns on a principal contour (*A*) and its neighbouring weak contour (*B*), which may correspond to a subsidiary maximum of the electron diffraction pattern. The stepped structure which is predicted in figure 6 can be seen between these

two moiré patterns. The thickness of the present crystal and some of the indices of the extinction contours are not known for the case of figures 15 to 17. But from the separations of subsidiary maxima of electron difiraction spots (see Hashimoto 1954; Uyeda *et al.* 1954) which are often observed in the electron diffraction pattern of Cu S film prepared under similar conditions, the thickness of the film is estimated to be 200 to 400 Å. As the thickness of the film $1/8q$ corresponds to 90 and 140 Å for 11·0 and 10·0 reflexions of Cu S crystal, the thicknesses of the double-layer films are given as 180 and 280 Å. Then the estimated thickness coincides with the thicknesses $1/8q \sim 2/8q$. The present theory, therefore, seems to explain essentially the present observation.

(*b*) *Parallel moiré patterns*

Figure 18, plate 8, which was taken by Bassett *et al.* (1958) is an electron microscopic image of a moiré pattern from a palladium single crystal grown epitaxially upon the (111) face of a gold single crystal. The pattern varies from one region to another owing to the variation in reflecting condition arising from buckling of the specimen. The brightnesses of the portions labelled *A* and *B* may suggest that they are in the exact Bragg reflecting position and far from it, respectively. Figures 8 and 9 suggest that no fringe is often observed for the palladium-gold film at the exact Bragg angle. For example, if the thicknesses of the films are the same and are equal to $3n/16q$, $4n/16q$, $n = 1, 2, \ldots$ (which correspond to 30 nÅ, 40 nÅ for the reflexion 022), no fringes and a rather dark band are observed at the exact Bragg reflecting position. Then there may be no fringes in the portion *A* due to its optimum thickness. Bassett *et al.* (1958) have pointed out that the observed value of the spacing of parallel moiré patterns show considerable deviation from the mean value, which differs by more than 10 % from the value calculated from the diffraction patterns. As was discussed in § 2(*d*), the spacing anomaly in parallel moiré patterns should be observed by the variation of the Bragg condition. The present theory can predict that if the crystals are bent or are not of uniform thickness, there can be up to a 50 % variation in spacing. In figure 18, it is possible to detect anomalies of spacing and intensity in the region between *A* and *B*. It is difficult to discuss all the anomalies quantitatively because of the presence of dislocations and the unknown thickness of the specimen. However, some of the anomalies of intensity and spacing in the region between *A* and *B* can be explained by the present theory.

(*c*) *Resolved lattice images of two crystals superposed*

Figure 19, plate 8, is an image of overlapping crystals of platinum phthalocyanine taken by Menter (1958). The two crystal lattice fringes of the $(20\bar{1})$ plane and a moiré pattern can be seen. The directions of the two crystal lattice fringes and the moiré pattern are indicated by arrows, *A*, *B* and *C*. It can clearly be seen that the crystal lattice fringe in the region of overlap is similar to that shown in figure 14. Though the thickness of each crystal is not known, by referring to the result shown in figure 14, it may be concluded that the crystal B is on the exit side for the electron wave. The present theory, therefore, seems to explain the present observation.

6. Conclusion

The present theory has explained the fine structure of the moiré pattern satisfactorily and, therefore, it seems to be essentially correct for the interpretation of the moiré pattern.

Dowell *et al.* (1956) shows that the rotation moiré pattern may represent the Patterson function. Cowley & Moodie (1959) derived this result from much more general consideration and discussed the possibility of structure analysis of the crystal by using the moiré pattern. According to the present theory, their conclusion holds when the crystals are set at the exact Bragg angle and the crystals are thin enough. In such cases, the intensity distribution of the moiré pattern is expressed from equation (2·47) as

$$I = A_g + BV_g^2 \cos 2\pi\epsilon \mathbf{g}\cdot\mathbf{r}, \tag{2·76}$$

where

$$A_g = 1 + \left(\frac{\pi}{\lambda E} Z V_g\right)^4,$$

$$B = -\frac{1}{2}\left(\frac{2\pi}{\lambda E} Z\right)^2.$$

If many sets of moiré patterns corresponding to $hk0$ reflexions are taken under the same condition and superposed at the original situation the integrated intensity distribution of the fringes is given by

$$P(xy) = \frac{1}{B}\left[B \sum_h \sum_k A_{hk} + \sum_h \sum_k |V_{hk}|^2 \cos 2\pi\{hx + ky\}\right]. \tag{2·77}$$

As $\sum_h \sum_k A_{hk}$ gives a uniform intensity distribution equation (2·77) gives in fact a Patterson distribution.

For a thick crystal, the approximation of equation (2·76) holds no longer. In such a case, it is necessary to obtain the corresponding fringes with amplitudes $|V_{hk0}|^2$ from the observed fringes of amplitudes $\frac{1}{2}\{(\sin 2\pi)\,(V_{hk0}/\lambda E)\}^2$ by using the method described at the conclusion in part I.

The authors would like to express their sincere thanks to Professor K. Tanaka and Professor R. Uyeda for encouragement and helpful discussion, and to Professor A. H. Cottrell, F.R.S., for his help in facilitating the publication of this paper. We would also like to acknowledge our thanks to Dr J. M. Cowley and Dr J. W. Menter for their interest and helpful discussions and to Dr J. W. Menter, Dr D. W. Pashley and Mr G. A. Bassett for providing copies of their micrographs.

References

Bassett, G. A., Menter, J. W. & Pashley, D. W. 1958 *Proc. Roy. Soc.* A, **246**, 345.
Bernard, R. & Pernoux, E. 1953 *C.R. Acad. Sci., Paris*, **236**, 187.
Bethe, H. A. 1928 *Ann. Phys., Lpz.*, **87**, 55.
Cowley, J. M. 1959 *Acta Cryst.* **12**, 367.
Cowley, J. M. & Moodie, A. F. 1959 *Acta Cryst.* **12**, 423.
Dawson, I. M. & Follet, E. A. C. 1959 *Proc. Roy. Soc.* A, **253**, 390.
Dowell, W. C. I., Farrant, J. L. & Rees, A. L. G. 1956 *Proc. 3rd Int. Conf. Electron Microscopy, London*, 1954, p. 279.
Dowell, W. C. I., Farrant, J. L. & Rees, A. L. G. 1957 *Electron Microscopy. Proc. First Regional Conference in Asia and Oceania, Tokyo*, 1956, p. 320.
Goodman, J. F. 1957 *Nature, Lond.* **180**, 425.
Hashimoto, H. 1954 *J. Phys. Soc. Japan*, **9**, 150.
Hashimoto, H. & Uyeda, R. 1957 *Acta Cryst.* **10**, 143.

PHILOSOPHICAL TRANSACTIONS OF THE ROYAL SOCIETY A MATHEMATICAL, PHYSICAL & ENGINEERING SCIENCES

Hashimoto, H. 1958 *J. Phys. Soc. Japan*, **13**, 534.
Hillier, J. 1954 *Nat. Bur. Stand. Circ.*, no. 527, Electron Physics, p. 413.
Izui, K. 1959 *J. Phys. Soc. Japan*, **14**, 1829.
Menter, J. W. 1958 *Phil. Mag. Suppl.* **7**, 299.
Mitsuishi, T., Nagasaki, H. & Uyeda, R. 1951 *Proc. Imp. Acad. Japan*, **27**, 86.
Möllenstedt, G. & Duker, H. 1953 *Phys. Verh.* **4**, 98.
Pashley, D. W., Menter, J. W. & Bassett, G. A. 1957 *Nature, Lond.* **179**, 752.
Rang, O. 1953 *Z. Phys.* **136**, 465.
Seki, Y. 1951 *J. Phys. Soc., Japan*, **6**, 534.
Seki, Y. 1953 *J. Phys. Soc., Japan*, **8**, 149.
Uyeda, R., Ichinokawa, T. & Fukano, Y. 1954 *Acta Cryst.* **7**, 216.

PHILOSOPHICAL TRANSACTIONS OF THE ROYAL SOCIETY A MATHEMATICAL, PHYSICAL & ENGINEERING SCIENCES

(15)

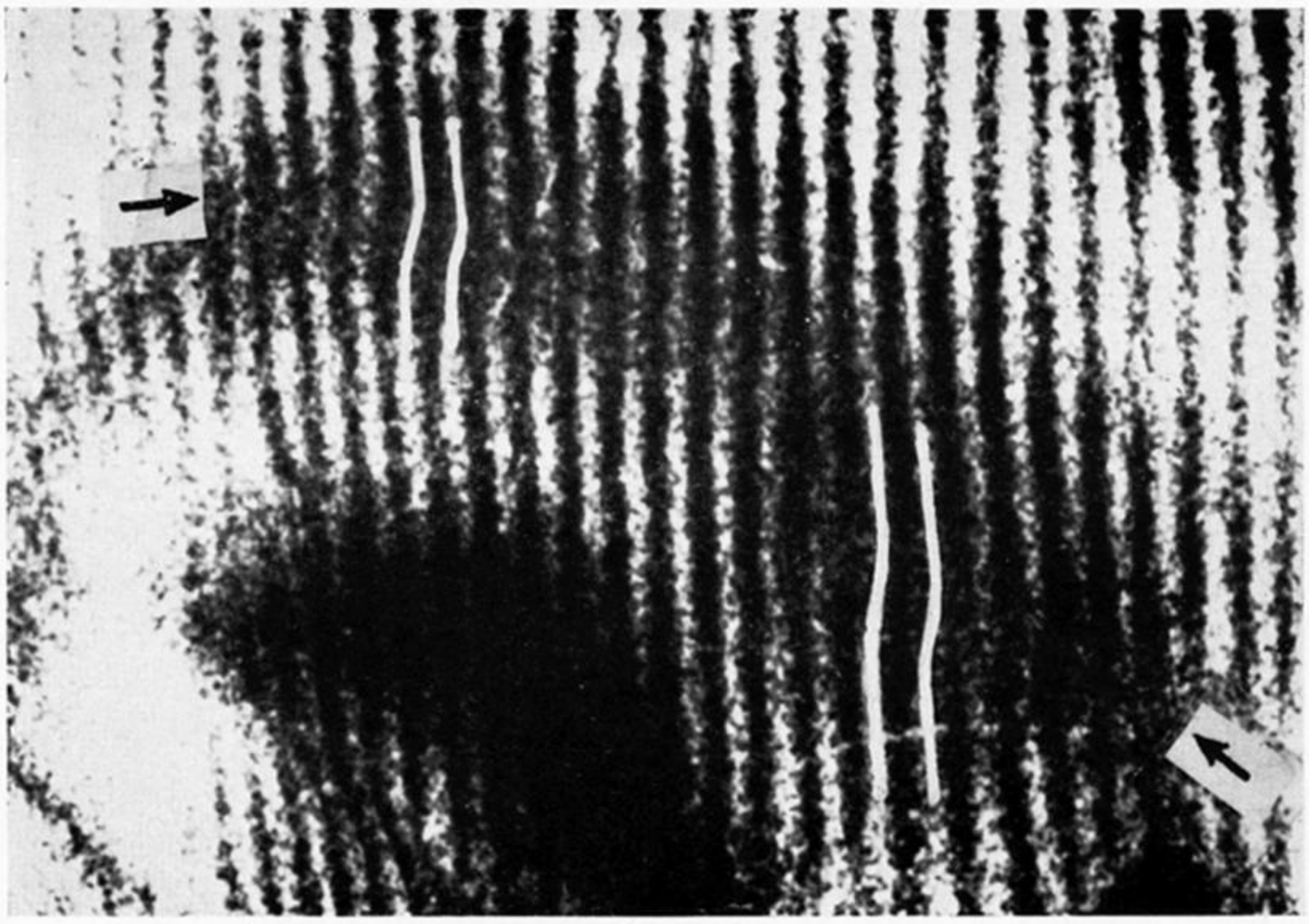

(16)

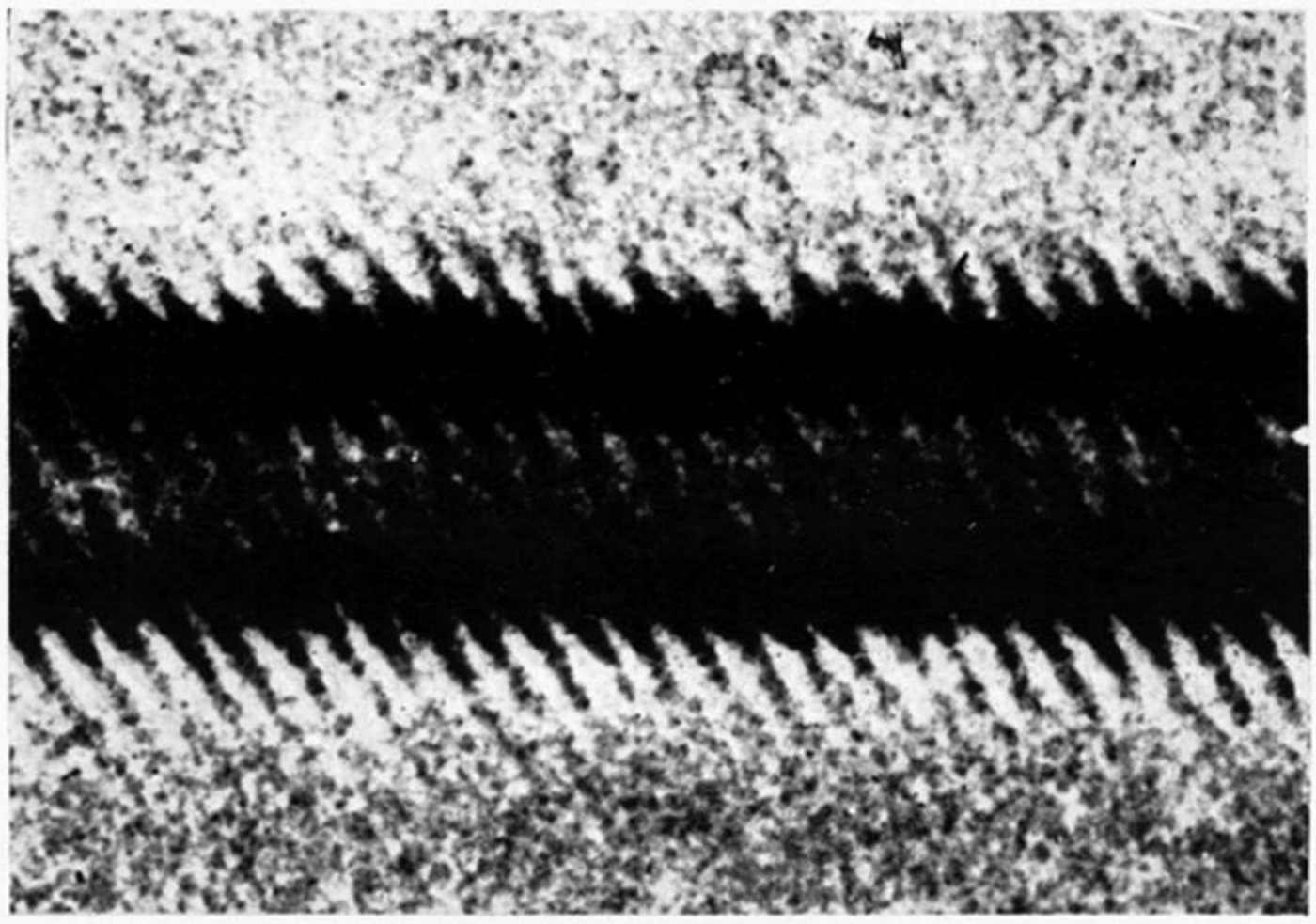

(17)

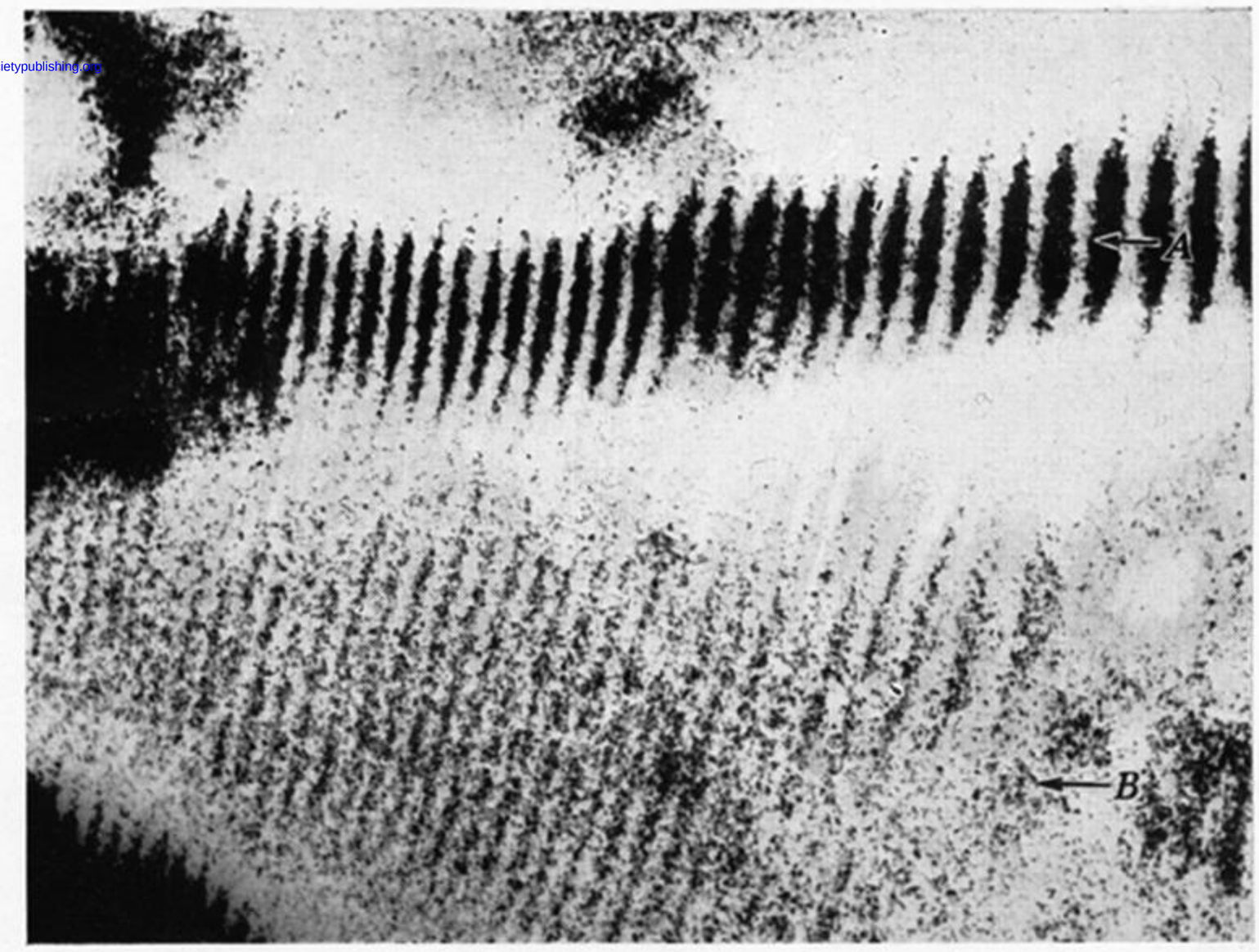

FIGURE 15. Moiré pattern of a cupric sulphide crystal showing the shift of the fringes near the centre of an extinction contour band. See marks ←. (Magn. × 400 000.)

FIGURE 16. Moiré patterns of cupric sulphide crystal on two extinction contour bands 10·0 and $\bar{1}0{\cdot}0$ showing the stepped structure between them. (Magn. × 400 000.)

FIGURE 17. Moiré patterns of a cupric sulphide crystal on a principal contour (*A*) and its neighbouring weak contours (*B*), showing the stepped structure between them. (Magn. × 400 000.)

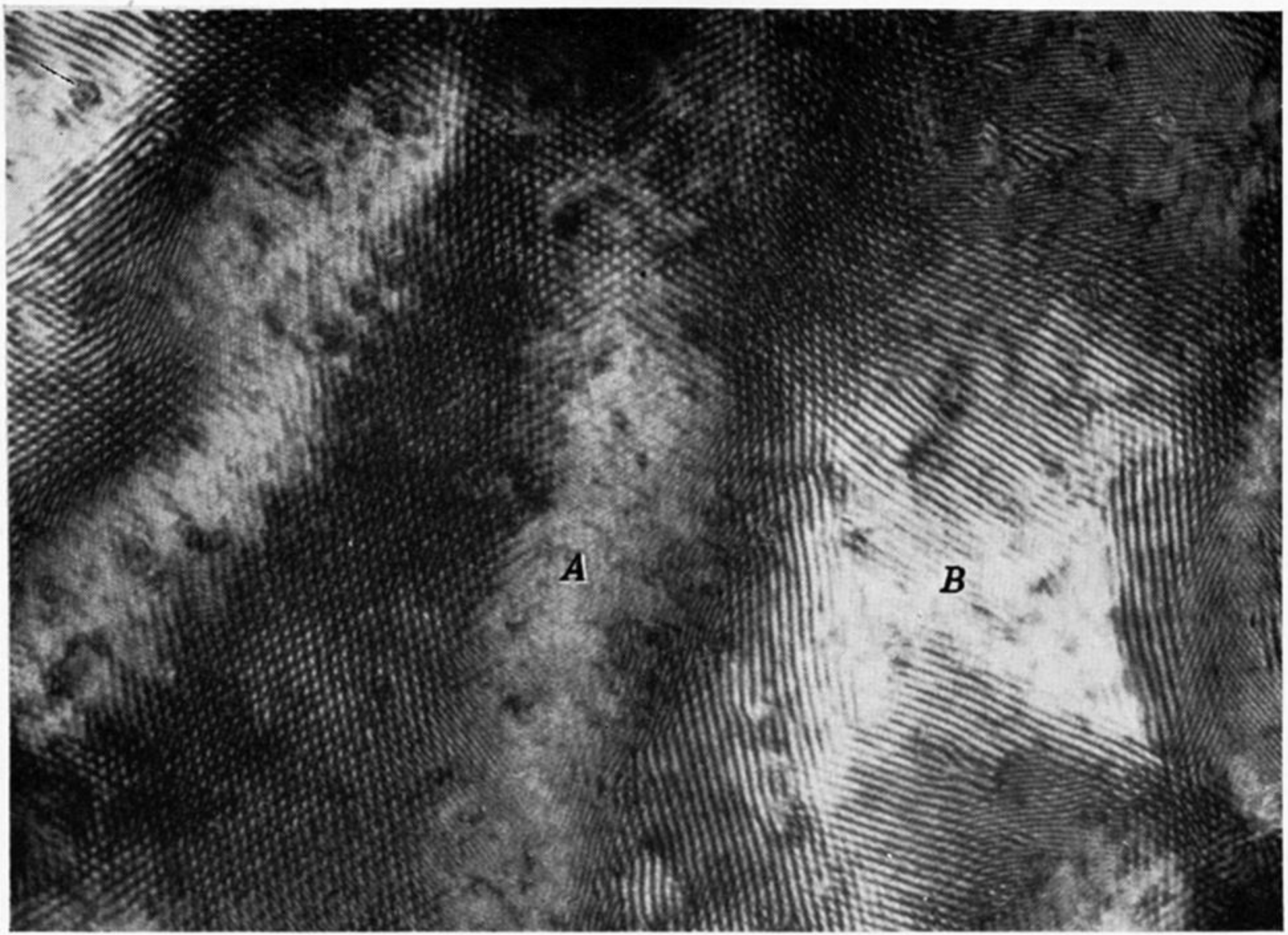

FIGURE 18. Moiré pattern from a specimen consisting of a palladium single crystal grown epitaxially upon a gold single crystal. (Magn. × 300 000.) (Courtesy Bassett, Menter & Pashley 1958.)

PHILOSOPHICAL TRANSACTIONS OF THE ROYAL SOCIETY A MATHEMATICAL, PHYSICAL & ENGINEERING SCIENCES

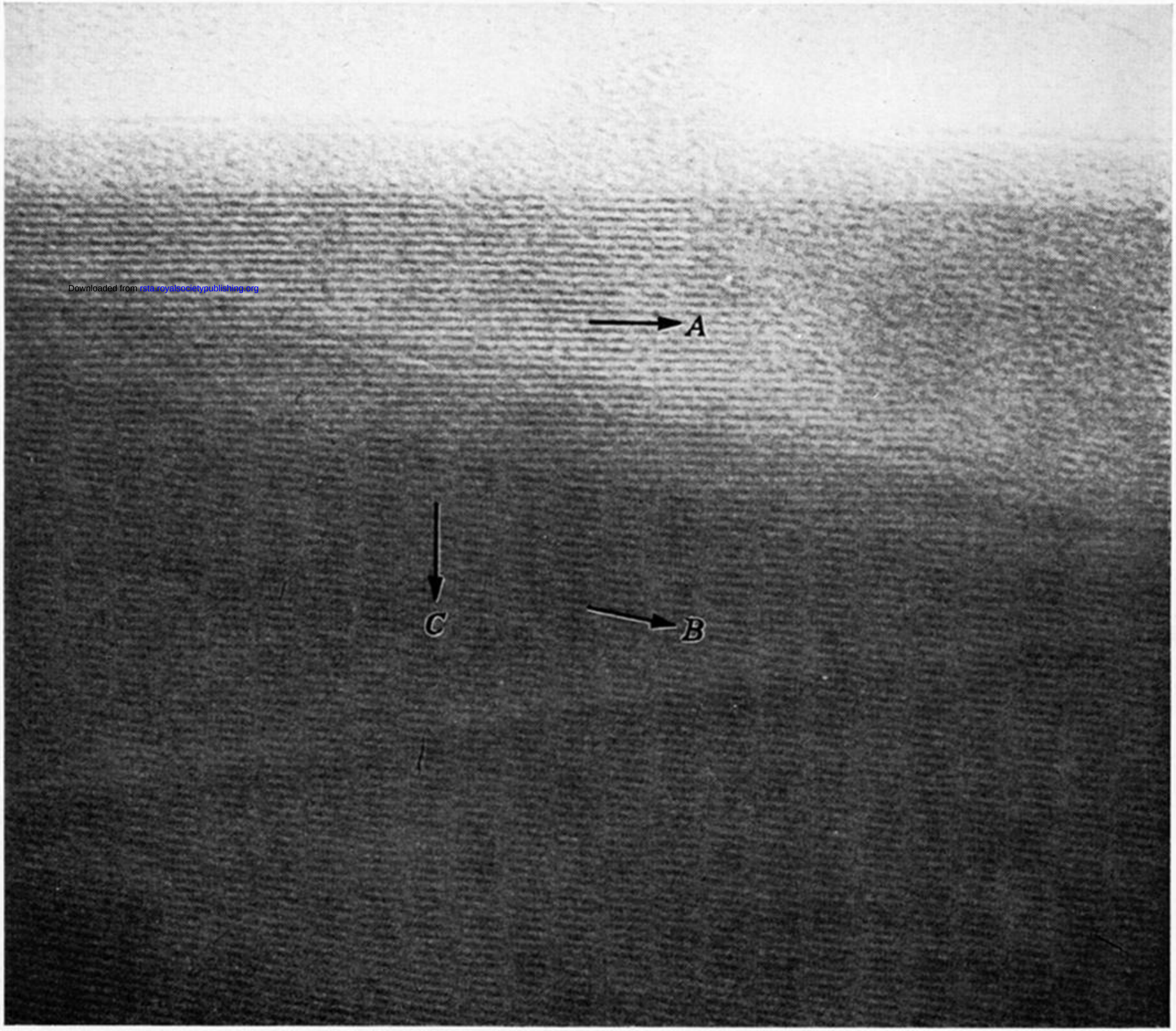

FIGURE 19. Overlapping crystals of platinum phthalocyanine showing crystal lattice fringes resolved and a moiré pattern formed in the region of overlap. (Magn. × 950 000.) (Courtesy Menter 1958.)

PHILOSOPHICAL TRANSACTIONS OF THE ROYAL SOCIETY A MATHEMATICAL, PHYSICAL & ENGINEERING SCIENCES